Impact of the Bowen Ratio on Surface-Layer Parameterizations of Heat, Moisture, and Turbulent Fluxes in Drylands

TEMPLE R. LEE,[a] SANDIP PAL,[b] TILDEN P. MEYERS,[c] PRAVEENA KRISHNAN,[a] BRIAN HIRTH,[d] MARK HEUER,[a,e] RICK D. SAYLOR,[a] JOHN KOCHENDORFER,[a] AND JOHN SCHROEDER[b,d]

[a] *NOAA/Air Resources Laboratory, Oak Ridge, Tennessee*
[b] *Atmospheric Science Group, Department of Geosciences, Texas Tech University, Lubbock, Texas*
[c] *NOAA/Air Resources Laboratory, Boulder, Colorado*
[d] *National Wind Institute, Texas Tech University, Lubbock, Texas*
[e] *Oak Ridge Associated Universities, Oak Ridge, Tennessee*

(Manuscript received 22 April 2024, in final form 24 January 2025, accepted 13 February 2025)

ABSTRACT: There is strong evidence that evaluating different parameterization schemes over diverse land surface forcings and surface-layer (SL) conditions will enhance our understanding of the physical processes required to improve the model parameterizations. Furthermore, shortcomings for representing SL heat, moisture, momentum, and turbulence using traditional parameterizations from Monin–Obukhov similarity theory (MOST) and the bulk Richardson approach are becoming well known within the scientific community. Overcoming the parameterizations' limitations requires evaluating the parameterizations across a range of land-cover types and meteorological conditions because the biosphere–atmosphere coupling is primarily linked to partitioning energy between sensible and latent heat fluxes. Recent studies over semiarid regions suggested that MOST better parameterized heat fluxes than the Richardson parameterizations, whereas the Richardson approach better parameterized kinematic and turbulence quantities. However, questions remain regarding whether the parameterizations' efficacy over drylands can be explained by physical parameters, such as the observed Bowen ratio (i.e., the ratio of the surface sensible heat flux to the surface latent heat flux). Addressing these questions allows one to more confidently use the parameterizations in land surface models. In this study, we used micrometeorological observations from two semiarid grassland sites, one in southeastern Arizona and a second in northwestern Texas, for a 3-yr period (1 January 2016–31 December 2018). We found that the heat flux, moisture flux, and turbulence parameterizations' efficacy do not vary with observed Bowen ratio. Furthermore, the MOST turbulence parameterizations sometimes performed better than the Richardson parameterizations, suggesting that caution is warranted particularly when applying the latter to semiarid regions.

SIGNIFICANCE STATEMENT: The proper parameterization of surface-layer processes is a crucial component of weather forecasting models. To improve the current suite of surface-layer parameterizations, they need to be evaluated across a range of conditions, ranging from very moist to very dry. Although this study found that the efficacy of surface-layer parameterizations varies little across these conditions, it represents an important step toward identifying the parameterizations' limitations in representing land–atmosphere exchanges. Understanding when these parameterizations perform well versus when their performance declines will help identify targeted areas for improvement and enhance their effectiveness in weather forecasting models.

KEYWORDS: Atmosphere–land interaction; Parameterization; Desert meteorology

1. Introduction

In the rapidly warming global climate of the twenty-first century, a comprehensive understanding of the surface energy balance (SEB) over different ecosystems remains a critical element for both numerical weather prediction (NWP) and climate models because of their poor representation of the relationships among land-cover and land-use changes, land–atmosphere feedback processes, and hydrological balance (Ripple et al. 2024). Many of uncertainties in the SEB closure and associated biosphere–atmosphere coupling arise because atmospheric boundary layer (ABL) parameterization schemes were often derived from empirical findings obtained over flat, horizontally homogeneous terrain (e.g., Kumar et al. 2006; Stiperski et al. 2019). For example, the shortcomings for representing surface-layer (SL) heat, moisture, momentum, and turbulent fluxes that use traditional parameterizations obtained from Monin–Obukhov similarity theory (MOST; Monin and Obukhov 1954) are well known within the scientific community and have been well documented in previous studies (e.g., Businger et al. 1971; Hicks 1978, 1981; Andreas and Hicks 2002; Detto et al. 2008; Salesky and Chamecki 2012; Pal et al. 2013; Pal and Haeffelin 2015; Sfyri et al. 2018; Markowski et al. 2019; Lee and Buban 2020; Sun et al. 2020; Stiperski and Calaf 2023; Lee et al. 2025). Limitations of MOST include self-correlation (e.g., Hicks 1978, 1981), the assumption of a horizontally homogeneous layer (e.g., Businger et al. 1971), and discrepancies between the stability functions for sensible and latent heat (e.g., Lamaud and Irvine 2006). Although these and other shortcomings

Corresponding author: Temple R. Lee, temple.lee@noaa.gov

DOI: 10.1175/JAMC-D-24-0075.1

have been identified over the past several decades, the scientific community has yet to remedy them. Therefore, alternative approaches have been proposed that use, for example, a different scaling variable instead of the Monin–Obukhov length scale. An alternative approach is to use a Richardson-based scaling approach (e.g., Dyer 1974; Byun 1990; Högström 1996; Meesters et al. 1997; Sorbjan 2010; Sorbjan and Grachev 2010; Lee and Buban 2020; Lee et al. 2019, 2021; Greene et al. 2022; Lee and Meyers 2023; Lee et al. 2023b). Richardson-based approaches have the advantage of reducing self-correlation present in MOST (e.g., Sorbjan 2006), provide continuity from unstable to stable regimes, and may also be better suited for very stable atmospheric regimes (e.g., Sorbjan 2010).

However, the Richardson-based scaling approach has not been systematically evaluated across a range of near-surface micrometeorological conditions and land surface types. Conducting this evaluation is important because very recent work (i.e., Lee et al. 2024) demonstrated, through the use of evaluations of the High-Resolution Rapid Refresh (HRRR) model (e.g., Benjamin et al. 2016; Dowell et al. 2022; James et al. 2022; Lee et al. 2023a), that the efficacy of NWP models varies as a function of different near-surface meteorological conditions and that model performance varies under different radiative regimes, soil moisture (SM) regimes, and near-surface heating rates. Lee et al. (2024) argued that meteorological regime-specific model verifications can help to identify specific areas where models do not perform well. Their work helps to provide motivation in the present study to evaluate the efficacy of MOST and Richardson-based SL parameterizations under an array of micrometeorological regimes. A systematic evaluation of the Richardson approach using multiyear datasets over different dryland ecosystems remains critical to facilitate the implementation of modified SL parameterizations into the next generation of convection-allowing operational weather forecasting models.

We argue that a framework similar to the one developed by Lee et al. (2024) needs to be employed when evaluating different SL parameterizations used in NWP models for representing heat, moisture, and momentum exchanges between the land surface and SL. However, only a few studies have so far evaluated SL parameterizations for heat and turbulent fluxes across a range of different near-surface micrometeorological regimes. Martí et al. (2022) found that traditional SL parameterizations from MOST have limitations under moist conditions. In contrast to the work by Martí et al. (2022), Lee et al. (2023b) reported that MOST SL parameterizations, as well as SL parameterizations using a Richardson-based scaling approach, have difficulty simulating SL fluxes in instances with large observed sensible heat fluxes.

The above difficulties, summarized by Martí et al. (2022) and Lee et al. (2023b), are particularly important over arid and semiarid regions, which we hereinafter refer to as drylands. Roughly three billion people live in drylands (e.g., Reynolds et al. 2007; Berg et al. 2016; Huang et al. 2017), and drylands occupy approximately 41% of terrestrial land surfaces globally (e.g., Prăvălie 2016). Because drylands are in general water-limited, sensible heat fluxes are oftentimes large over drylands, and the sensible heat fluxes well exceed the latent heat fluxes. Consequently, the Bowen ratio β, which is defined as the ratio of the surface sensible heat flux H to the latent heat flux (LE) (e.g., Sverdrup 1943; Lewis 1995), is typically large, but β is highly sensitive to soil moisture (e.g., Krishnan et al. 2012; Liu et al. 2024). Thus, low-precipitation regimes and water availability significantly impact dryland ecosystems and should be included in SL parameterizations, especially those for water and carbon fluxes, in these areas (e.g., Kannenberg et al. 2024). Additionally, the heat flux partitioning (via β) has a large influence on the near-surface meteorological conditions, which affect the mean and turbulent structure of the ABL, which, in turn, impacts convection initiation and cloud formation (Findell and Eltahir 2003; Bhowmick and Parker 2018). Other studies showed that β is also sensitive to surface heterogeneity, soil properties, and advective effects (e.g., Friedrich et al. 2000).

Furthermore, drylands have a larger sensitivity to climate warming than the global average (Huang et al. 2017) and thus are more sensitive to increases in aridification than other areas of the world, which is caused by the redistribution of global precipitation under a changing climate (e.g., Konapala et al. 2020). Additionally, a holistic approach to evaluate NWP models for drylands remains underdeveloped due to a lack of measurements over these areas and because comparatively little attention has been given to the study of ABL processes over drylands (Mauder et al. 2021; Pal et al. 2021). An overview of the state-of-the-art observations and simulations of ABL thermodynamics was reported for many different environments (i.e., urban, coastal, marine, complex terrain, polar regions, and across interfaces) within a recent (National Academies of Sciences, Engineering, and Medicine 2018) workshop on the "Future of ABL" and in NASA's "ABL Incubation Study Team Report" (Teixeira et al. 2021), but discussions of ABL processes over drylands were absent. Because of the relative lack of study of drylands as compared with other environments, NWP models can have large errors over drylands, which exacerbates the risks to the billions of people residing in these areas.

In the present study, we evaluated the efficacy of the MOST and Richardson-based parameterizations across different near-surface micrometeorological regimes that are typically found in drylands. We distinguished among different near-surface regimes by calculating β using measurements from Audubon in southeastern Arizona and the Reese Technology Center (RTC) in northwestern Texas. Although both sites are located in the drylands of the southwestern United States and have a semiarid climate, the sites themselves are uniquely different. Audubon is annually impacted by the North American monsoon, whereas the RTC is largely unaffected by the North American monsoon but is instead affected by synoptic- to regional-scale weather patterns (e.g., fronts, drylines) due to the Gulf of Mexico and the westward extension of the Bermuda high (e.g., Clark et al. 2022; Anand and Pal 2023; Pal et al. 2024). We used observations from both Audubon and RTC to calculate β. Doing so allowed for us to evaluate the efficacy of MOST and Richardson SL parameterizations for H, LE, friction velocity u_*, and turbulent

kinetic energy (TKE) for a wide range of observed β over a 3-yr period (i.e., 1 January 2016 through 31 December 2018). Observations from Audubon and RTC had been used by Lee et al. (2023b) to evaluate the efficacy of different SL parameterizations for sensible heat flux, friction velocity, and turbulent kinetic energy for only 1 year of observations. However, Lee et al. (2023b) did not evaluate the efficacy of latent flux parameterizations, and it was unclear how varying near-surface conditions affected the SL parameterizations' efficacy. In the next section, we summarize the derivations of the MOST and Richardson SL parameterizations used to calculate SL heat, moisture, momentum, and turbulent fluxes prior to discussing the datasets that we used to evaluate the parameterizations' efficacy as a function of varying β.

2. MOST and Richardson parameterizations for SL heat, moisture, and turbulent fluxes

a. *MOST parameterizations*

The MOST and Richardson parameterizations for H, LE, u_*, and TKE have been derived and discussed in previous works (i.e., Jiménez et al. 2012; Lee et al. 2021; Lee and Meyers 2023). Thus, these parameterizations are only briefly summarized here. In MOST, u_* is computed as

$$u_* = \frac{\kappa U}{\left[\ln\left(\frac{z-d}{z_0}\right) - \psi_m\left(\frac{z-d}{L}\right) + \psi_m\left(\frac{z_0}{L}\right)\right]}. \tag{1}$$

In the above equation, κ and U are the von Kármán constant and horizontal wind speed, respectively; z, d, z_0, and L is the height, zero-plane displacement, surface roughness length, and Monin–Obukhov length scale, respectively; and ψ_m is the momentum similarity function that varies as a function of atmospheric stability. In Eq. (1), L is defined as

$$L = -\frac{\overline{\theta}_v u_*^3}{\kappa g \overline{w'\theta'_v}}. \tag{2}$$

In the above equation, $\overline{\theta}_v$, g, and $\overline{w'\theta'_v}$ are the mean virtual potential temperature, gravitational acceleration, and kinematic heat flux, respectively.

The parameterized u_*, which we term u'_*, is then used in the MOST parameterization for H and LE:

$$H = -\frac{\kappa \Delta\theta u'_* \rho c_p}{\left[\ln\left(\frac{z_2-d}{z_1-d}\right) - \psi_h\left(\frac{z_2-d}{L}\right) + \psi_h\left(\frac{z_1-d}{L}\right)\right]}, \tag{3a}$$

$$\mathrm{LE} = -\frac{\Delta q \kappa u'_* \rho L_v}{\left[\ln\left(\frac{z_2-d}{z_1-d}\right) - \psi_q\left(\frac{z_2-d}{L}\right) + \psi_q\left(\frac{z_1-d}{L}\right)\right]}. \tag{3b}$$

Here, $\Delta\theta$, Δq, ρ, c_p, and L_v are the potential temperature gradient, specific humidity gradient, air density, specific heat of air, and latent heat of vaporization, respectively; z_1 and z_2 are the heights at which the potential temperature and specific humidity are measured above the ground; and ψ_h and ψ_q are the heat and moisture similarity functions, respectively, that are analogous to ψ_m, and also depend upon atmospheric stability.

The three components of TKE, i.e., σ_u, σ_v, and σ_w, which are the standard deviations in the u (i.e., horizontal), v (i.e., meridional), and w (i.e., vertical) wind components, respectively, are parameterized as a function of u'_* and ζ [where $\zeta = (z-d)/L$] following Lee and Meyers (2023):

$$\sigma_{u,v,w} = \begin{cases} u'_* \alpha_{\sigma_{u,v,w}} (1 - \beta_{\sigma_{u,v,w}} \zeta)^{1/3}, & \zeta < 0 \\ u'_* \mu_{\sigma_{u,v,w}} \exp(\nu_{\sigma_{u,v,w}} \zeta), & \zeta > 0 \end{cases}. \tag{4}$$

In Eq. (4), $\alpha_{\sigma_{u,v,w}}$, $\beta_{\sigma_{u,v,w}}$, $\mu_{\sigma_{u,v,w}}$, and $\nu_{\sigma_{u,v,w}}$ are the empirically derived fitting coefficients from Lee and Meyers (2023). Once $\sigma_{u,v,w}$ has been computed, the TKE is computed as a function of parameterized values for σ_u, σ_v, and σ_w, which we term σ'_u, σ'_v, and σ'_w, respectively, via Eq. (5):

$$\mathrm{TKE} = 0.5[(\sigma'_u)^2 + (\sigma'_v)^2 + (\sigma'_w)^2]. \tag{5}$$

b. *Ri_b parameterizations*

As described in, for example, Stull (1988) and Lee and Buban (2020), the bulk Richardson number Ri_b represents the ratio of the consumption of turbulence to the shear production of turbulence and is computed as

$$\mathrm{Ri}_b = \frac{g\Delta\overline{\theta}_v \Delta z}{\overline{\theta}_v[(\Delta\overline{u})^2 + (\Delta\overline{v})^2]}. \tag{6}$$

In Eq. (6), u and v are the mean horizontal and meridional components of the wind, respectively, computed between two sampling heights, and the remaining variables have been defined previously. The specific sampling heights used are noted in the next section.

From Lee et al. (2021), u_* is parameterized as a function of Ri_b whereby

$$u_* = UC_u(\mathrm{Ri}_b). \tag{7}$$

Here, C_u is the friction-transfer coefficient that is a function of Ri_b and like the MOST parameterizations also depends upon atmospheric stability.

The terms H and LE are also functions of Ri_b and Ri_b-parameterized u_* (which we term u''_* to eliminate any potential confusion with the MOST-parameterized u_* represented as u'_*), whereby

$$H = -\Delta\theta u''_* C_t(\mathrm{Ri}_b) c_p \rho, \tag{8a}$$

$$\mathrm{LE} = -\Delta q u''_* C_r(\mathrm{Ri}_b) \rho L_v. \tag{8b}$$

In the above equations, $C_t(\mathrm{Ri}_b)$ and $C_r(\mathrm{Ri}_b)$ are the similarity functions for heat transfer and moisture transfer, respectively, and the remaining variables have been defined previously. Following Lee et al. (2021), $C_{u,t,r}$ has the following form for different Ri_b (i.e., whether $\mathrm{Ri}_b < 0$ or $\mathrm{Ri}_b > 0$) and is a function of the fitting coefficients $\lambda_{u,t,r}$, $\omega_{u,t,r}$, $\chi_{u,t,r}$, and $\gamma_{u,t,r}$:

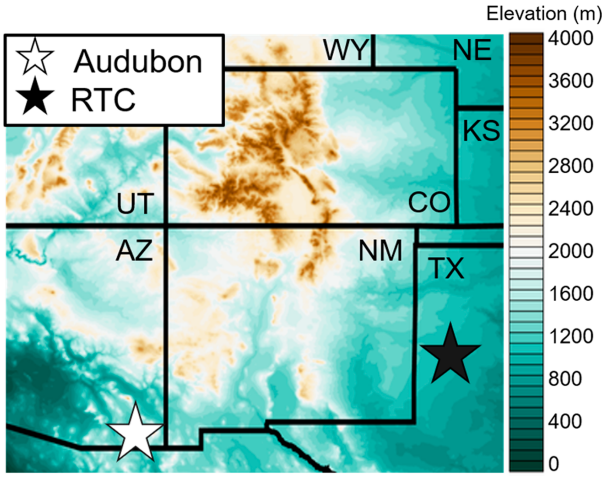

FIG. 1. Location of Audubon (white star) and the RTC (black star) in the Southwest United States relative to other states (labeled) in the region. The topography data were obtained from the Parameter-Elevation Regressions on Independent Slopes Model (PRISM) and have a 30-arc-s resolution.

$$C_{u,t,r} = \begin{cases} \lambda_{u,t,r}(1 - \omega_{u,t,r}\mathrm{Ri}_b)^{1/3}, & \mathrm{Ri}_b < 0 \\ \chi_{u,t,r}\exp(\gamma_{u,t,r}\mathrm{Ri}_b), & \mathrm{Ri}_b > 0 \end{cases}. \quad (9)$$

Just as the MOST TKE parameterizations are a function of MOST-parameterized u_* (i.e., u_*') and ζ, the Ri_b TKE parameterizations are a function of u_*'' and Ri_b:

$$\sigma_{u,v,w} = \begin{cases} u_*''\lambda_{\sigma_{u,v,w}}(1 - \omega_{\sigma_{u,v,w}}\mathrm{Ri}_b)^{1/3}, & \mathrm{Ri}_b < 0 \\ u_*''\chi_{\sigma_{u,v,w}}\exp(\gamma_{\sigma_{u,v,w}}\mathrm{Ri}_b), & \mathrm{Ri}_b > 0 \end{cases}. \quad (10)$$

3. Observations

a. Study sites

We used observations from two micrometeorological towers in the southwestern United States: a 10-m tower in southeastern Arizona at Audubon [31.59°N, 110.51°W, 1473 m above mean sea level (MSL)] and a second 200-m tower in northwestern Texas near Lubbock at the RTC (33.61°N, 102.05°W, 1020 m MSL) (Fig. 1). The sites themselves and the datasets from these two sites have been described in previous works (i.e., Krishnan et al. 2012; Hamel 2022; Lee et al. 2023b) and thus are only briefly summarized in this section.

1) ARIZONA SITE

The Audubon semiarid grassland site in Arizona (Meyers 2016) is a part of the AmeriFlux network (Novick et al. 2018; Baldocchi et al. 2024) and of the NOAA Air Resources Laboratory Atmospheric Turbulence and Diffusion Division's Surface Energy Budget Network. The vegetation at Audubon is a native short-grass prairie, and the soil consists largely of well-draining sandy clay that is mixed with gravel (see e.g., Krishnan et al. 2012 for more details). The vegetation height typically ranges from about 40 to 70 cm in a given year (Lee et al. 2023b). In this study, we used a mean of these values (i.e., 0.55 cm) for the canopy height h_c and used $(2/3)h_c$ and $(1/10)h_c$ for d and z_0, respectively, in the equations for the MOST parameterizations discussed in section 2.

Whereas on-site flux and meteorological measurements began at Audubon in 2002, in the present study, we used data obtained from the site between 1 January 2016 and 31 December 2018 because this time period had the most complete data record of measurements at both Audubon and RTC. All instruments were well calibrated to ensure a high-quality dataset to evaluate the parameterizations. Most critical to this study are the on-site turbulence observations, which were obtained using a three-axis sonic anemometer (Model 81000 V, R. M. Young) that sampled at 10 Hz at 10 m above ground level (AGL) and was used to compute H, u_*, and TKE. Observations from an open-path infrared gas analyzer (model LI-7500, LI-COR Inc., Lincoln, Nebraska), also installed at 10 m AGL and using a 10-Hz sampling frequency, were used to compute LE. Ground heat flux G was derived using the soil temperature gradient following the approach in Sauer and Horton (2005). More details about the approach we used to compute the heat and turbulent fluxes appear in section 4.

Temperature observations at 1.5 and 8.5 m AGL were obtained using platinum resistance thermometers (Thermometrics Corp. PRT, Northridge, California), which have an accuracy of $<\pm 0.3°$. Two-dimensional wind observations at 2.5 and 9.5 m AGL were obtained using R. M. Young 05103 anemometers (R. M. Young Co., Traverse City, Michigan), which have an accuracy of ± 0.3 m s^{-1} and $\pm 3°$ for wind speed and wind direction, respectively. The temperature and wind observations were used to calculate the vertical gradients in the equation for Ri_b [cf. Eq. (6)].

2) TEXAS SITE

We used data from the RTC obtained over a 3-yr period between 1 January 2016 and 31 December 2018. The areas surrounding the site are characterized by wild grasses that have a mean height of about 20 cm. As we did for Audubon, we used $(2/3)h_c$ and $(1/10)h_c$ for d and z_0, respectively. According to the U.S. Geological Survey National Land Cover Database (NLCD; Jin et al. 2023), the vegetation in the region is mainly shrub–scrub and grasslands–herbaceous, whereas the soil is characterized by Acuff loam (i.e., very deep, well-drained, and moderately permeable soils) and has the taxonomic class of fine-loamy, mixed, superactive.

Although there are 10 sampling heights along the tower at the Reese Technology Center that extend upward to 200 m AGL, to maintain consistency with Audubon, we used only the observations from ~10 m AGL. The observations needed to compute H, LE, u_*, and TKE were obtained from a Gill R3-50 sonic anemometer and an R. M. Young 43182 V temperature/humidity sensor that sampled at 50 Hz (e.g., Hamel 2022; Lee et al. 2023b) and installed at 10.1 m AGL. The sonic anemometer has an accuracy of <1% root-mean-square (RMS) and

$<\pm 1°$ for wind speed and direction, respectively, whereas the temperature/humidity sensor has a temperature accuracy of ± 0.3°C and $\pm 1\%$ for relative humidity. We used the observations from 10.1 to 4.1 m AGL to calculate the vertical gradients in Eq. (6) for Ri_b.

b. Ancillary observations

Additional supporting near-surface meteorological measurements were used to place the Audubon and RTC observations from 2016 through 2018 into a climatological context. To this end, for Audubon, we used temperature and precipitation observations obtained from the collocated U.S. Climate Reference Network site (e.g., Diamond et al. 2013).

To provide climatological context for the RTC observations, we used long-term observations obtained from the West Texas Mesonet (WTM). The WTM site (33.608°N, 102.046°W, 1019 m MSL) is located approximately 530 m southeast of the RTC tower and has observations of wind speed 2 and 10 m AGL; air temperature 1.5, 2 m, and 9 m AGL; relative humidity 1.5 m AGL; atmospheric pressure; incoming shortwave radiation; and soil water content 5, 20, 60, and 75 cm below the surface. More details about the WTM can be found in, e.g., Schroeder et al. (2005). We also used observations obtained from the Automatic Station Observing System station at Lubbock International Airport, which is located approximately 20 km east-northeast of the RTC.

4. Methods

a. Data filtering

The high-frequency measurements (i.e., the 10-Hz datasets from Audubon and the 50-Hz datasets from RTC) were used to compute 30-min H, LE, u_*, and TKE by implementing the eddy covariance technique. The eddy covariance technique has been well-described in previous works, and its uncertainties are discussed in Massman and Lee (2002), Billesbach (2011), and Schmidt et al. (2012). In the present study, we applied standard despiking approaches and coordinate rotations, and we corrected LE for density effects using the Webb–Pearman–Leuning correction (e.g., Webb et al. 1980) following Meyers (2001) and Meyers and Baldocchi (2005) prior to computing the fluxes and turbulence statistics.

Following Lee et al. (2023b), for the RTC only, we removed the 30-min fluxes and turbulence statistics when the 30-min mean wind direction was between 110° and 170°. Filtering data from this sector was essential to remove the impacts of the wake of the tower and the wakes from the nearby wind turbines, which are located about 2 km away from the tower, on the turbulence measurements (Kelley and Ennis 2016; Lee et al. 2023b).

Once we computed the 30-min H, LE, u_*, and TKE, following Lee et al. (2023b), we removed physically unrealistic values from both sites, which we defined as $H < -200$ W m^{-2} or $H > 800$ W m^{-2}; LE < -200 W m^{-2} or LE > 800 W m^{-2}; $u_* < 0$ m s^{-1} or $u_* > 2$ m s^{-1}; and TKE < 0 m^2 s^{-2} or TKE > 10 m^2 s^{-2}. The removal of 30-min periods with missing data, as well as 30-min periods with physically unrealistic values, resulted in 93%, 85%, 94%, and 99% of the data being available for H, LE, u_*, and TKE, respectively, at Audubon. At the RTC, the data completion for H, LE, u_*, and TKE was 70%, 69%, 58%, and 70%, respectively, over the 3-yr study period following the removal of 1) erroneous 30-min fluxes and turbulence statistics and 2) 30-min periods when the 30-min wind direction was between 110° and 170°.

b. Determination of Bowen ratio ranges

In past work, it was demonstrated that regional-scale domain-average single-value β, without considering the temporal variability on diverse time scales (i.e., synoptic, subseasonal, and seasonal), can cause significant errors in NWP model forecasts because a large set of atmospheric and surface conditions (e.g., soil moisture memory and associated precipitation–soil moisture interactions, soil type, surface heterogeneity, etc.) cumulatively impact β (e.g., Friedrich et al. 2000; Martínez-Fernández et al. 2021). Thus, it is of paramount interest for the scientific community to explore the dependence of parameterizations for a diverse range of observed β over dryland ecosystems. To this end, to evaluate the MOST and Ri_b parameterizations across a range of near-surface conditions, we used the observed β from both sites. Because of errors associated with computing β during the nighttime, we restricted our analyses to observations sampled between 0800 and 1600 LST at each site. Note that, at Audubon and RTC, LST = UTC – 7 and LST = UTC – 6, respectively. We note that, although surface heterogeneity on the upwind side can potentially affect SEB closure, we did not have the appropriate measurements to investigate the impact of spatial heterogeneity in the land surface cover on our findings, as was reported in previous studies (e.g., Panin and Tetzlaff 1999).

Over the 3-yr period of interest, the daily mean β (computed between 0800 and 1600 LST for each day within the 3-yr period of interest) was larger at the RTC than at Audubon (Fig. 2). Furthermore, β exhibited more seasonality at Audubon (e.g., higher β in winter than in summer) than at the RTC due to the North American monsoon, which occurs annually at Audubon. However, the monsoon's impacts are largely absent at RTC. For instance, in the premonsoon months at Audubon, β was fairly constant but exhibits a marked decrease in early summer with the monsoon onset, which began in late June in 2016 and a couple of weeks later in 2017 and 2018, resulting in rapid vegetation growth at the site (e.g., Krishnan et al. 2012).

To obtain a range of conditions, we evaluated the H, LE, u_*, and TKE parameterizations across five different β quintiles at both sites to sample a wide range of near-surface micrometeorological conditions spanning from very low values of β (i.e., moist surface conditions) to very high values of β (i.e., dry surface conditions). Using the empirical findings based on the frequency distribution analyses of β for the entire measurement periods over both sites (Figs. 2b,d), we defined five different β regimes at each site as

I. <20th percentile of β
II. 20th–40th percentile of β
III. 40th–60th percentile of β
IV. 60th–80th percentile of β
V. >80th percentile of β

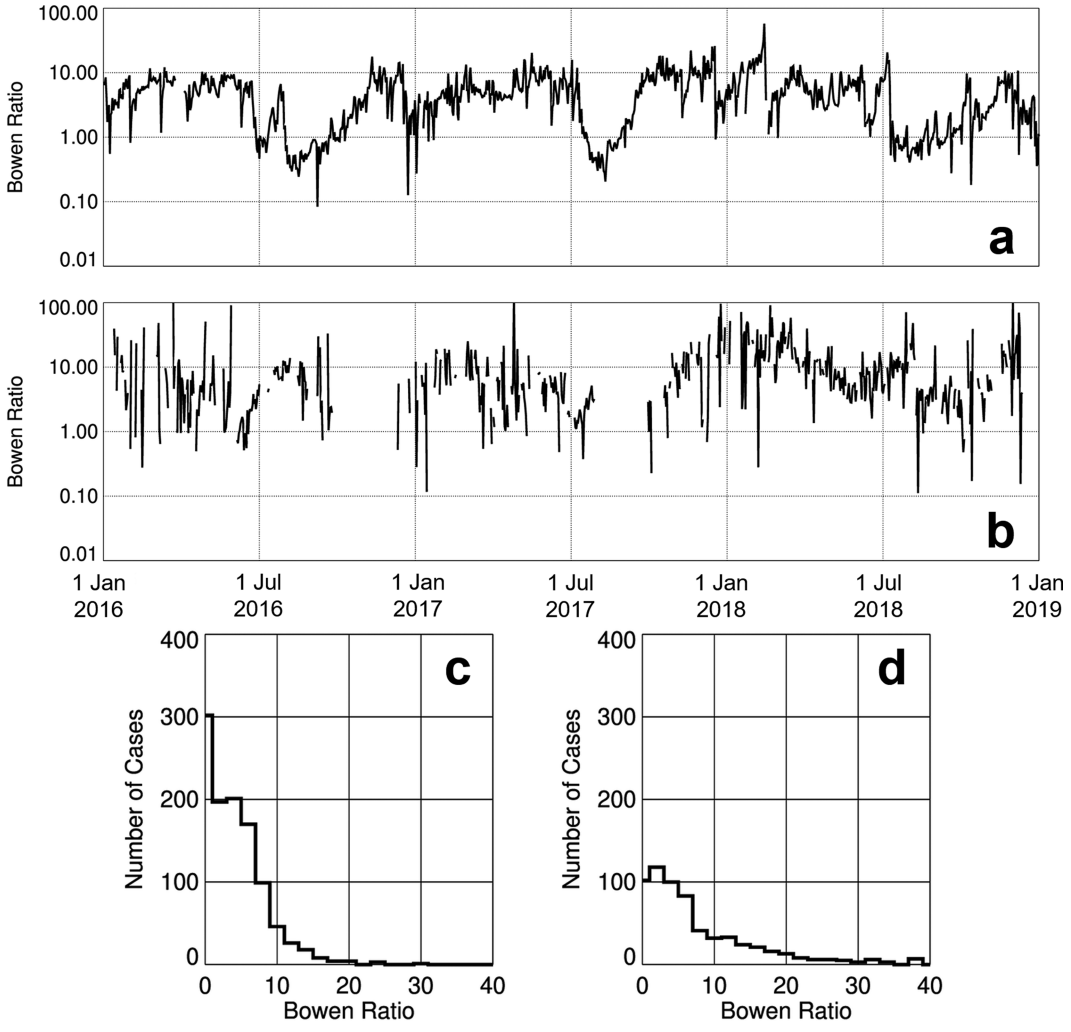

FIG. 2. Time series of mean daytime β, computed between 0800 and 1600 LST, at 10 m AGL at (a) Audubon and (b) RTC. Note the y axis in (a) and (b) has a logarithmic scale, and there are missing LE data in late 2016 and 2017 which result in gaps in the time series of β at the RTC [cf. (b)]. (c)(d) The histograms of the mean daytime β at 10 m AGL computed between 0800 and 1600 LST at Audubon and RTC, respectively.

The different β quintiles at Audubon and RTC are summarized in Tables 1 and 2, respectively. Bowen ratios were considerably lower at Audubon than at the RTC; the median daily β over the smallest β quintile (i.e., moist conditions) during the study period at Audubon was 0.74 but was 1.47 at the RTC. Despite having higher values of β, SM was oftentimes larger at the RTC (Fig. 3). Over the smallest β quintile, the 10-cm SM (5-cm SM) at Audubon (RTC) was 0.146 $m^3\ m^{-3}$ (0.220 $m^3\ m^{-3}$). We note that for higher SM, β at the RTC had larger values (Fig. 3b). In general, in addition to SM, β is

TABLE 1. Minimum, median, and maximum daily β (i.e., β_{min}, β_{med}, and β_{max}, respectively), and the minimum, median, and maximum daily 10-cm SM (i.e., SM_{min}, SM_{med}, and SM_{max}, respectively) at Audubon, illustrating a range of near-surface micrometeorological conditions ranging from very moist to very dry surface conditions over the five β regimes (i.e., I, II, III, IV, and V). Please see the text (i.e., section 4b) and the associated reference (i.e., Mauder et al. 2020) for a note regarding the high β values.

β regime	β percentile	β_{min}	β_{med}	β_{max}	SM_{min} ($m^3\ m^{-3}$)	SM_{med} ($m^3\ m^{-3}$)	SM_{max} ($m^3\ m^{-3}$)
I	<20th	0.1	0.8	1.3	0.057	0.145	0.264
II	20th–40th	1.4	2.4	3.6	0.031	0.098	0.248
III	40th–60th	3.6	4.7	5.7	0.026	0.074	0.222
IV	60th–80th	5.7	7.0	8.3	0.026	0.058	0.173
V	>80th	8.4	10.9	56.7	0.028	0.049	0.150

TABLE 2. As in Table 1, but for RTC.

β regime	β percentile	β_{min}	β_{med}	β_{max}	SM_{min} (m^3 m^{-3})	SM_{med} (m^3 m^{-3})	SM_{max} (m^3 m^{-3})
I	<20th	0.1	1.5	2.4	0.099	0.221	0.379
II	20th–40th	2.4	3.5	4.6	0.110	0.181	0.357
III	40th–60th	4.6	6.1	7.6	0.103	0.164	0.322
IV	60th–80th	7.6	10.7	14.5	0.099	0.136	0.346
V	>80th	14.6	23.0	96.4	0.099	0.141	0.364

affected by multiple other factors including soil type (e.g., the ratio of resistances between the atmosphere and soil pores), atmospheric moisture and stability, and near-surface temperature (e.g., Zhuojia and Pielke 1995). Furthermore, the interactions among these factors are oftentimes nonlinear. Additionally, other researchers have found that upstream near-surface atmospheric conditions also impact β at a given site (Friedrich et al. 2000). The results here suggest that, in addition to the low precipitation, stark aridity, and high winds in the region, the presence of gravel particles in the soil could store water themselves and lead to a reduction in the amount of water stored within the soil.

Over the largest β quintile (i.e., dry conditions), the median daily β at Audubon was 10.16 but was 22.99 at 10 m AGL at the RTC. SM was correspondingly lower at both sites in the highest β quintile; 10-cm SM at (5-cm SM) Audubon (RTC) in the largest β quintile was 0.046 m^3 m^{-3} (0.141 m^3 m^{-3}) due to the inverse relationship between SM and β, which is summarized in Fig. 3, and shows that SM approaches the wilting point when β is large. The largest β values at the RTC occurred on days when the mean daytime observed H was quite small (i.e., ~10 W m^{-2}), and the mean daytime LE was <1 W m^{-2} (cf. Table 2). The small values of H and LE are not very significative (e.g., Mauder et al. 2020) and likely result in larger errors in β than scenarios in which the observed surface fluxes are much higher.

Having determined different β quintiles at each site, we evaluated the efficacy of the different parameterizations as a function of β by computing the mean bias error (MBE), root-mean-square error (RMSE), and coefficient of regression R^2 between the parameterized and observed values of H, LE, u_*, and TKE at both sites during the measurement periods. Hereinafter, the MBE represents the difference between the parameterized and observed value and, for brevity, is abbreviated as δH, δLE, δu_*, and δTKE for H, LE, u_*, and TKE, respectively.

c. *Evaluation of parameterization efficacy when $\beta < 1$ and $\beta > 1$*

Given the different β ranges at Audubon and at the RTC (cf. section 4b), to evaluate further the efficacy of the MOST and Ri_b parameterizations, we differentiated between instances in which $\beta < 1$ and $\beta > 1$. We then determined the mean cycle in δH, δLE, δu_*, and δTKE for the MOST and Ri_b parameterizations at both Audubon and at the RTC, and we discuss these results in section 5e.

5. Results

a. *Overview of on-site meteorological conditions during period of interest*

1) ARIZONA SITE

During the 3-yr study period at Audubon, mean incoming shortwave radiation, computed between 0800 and 1600 LST,

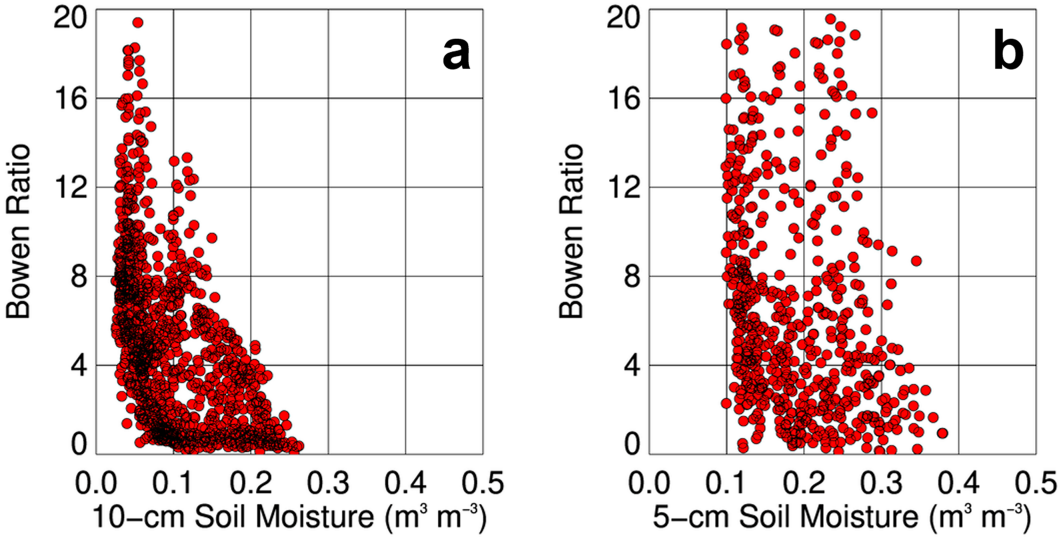

FIG. 3. (a) Bowen ratio as a function of 10-cm mean daytime (0800–1600) SM at Audubon and (b) Bowen ratio as a function of 5-cm mean daytime (0800–1600) SM at the RTC.

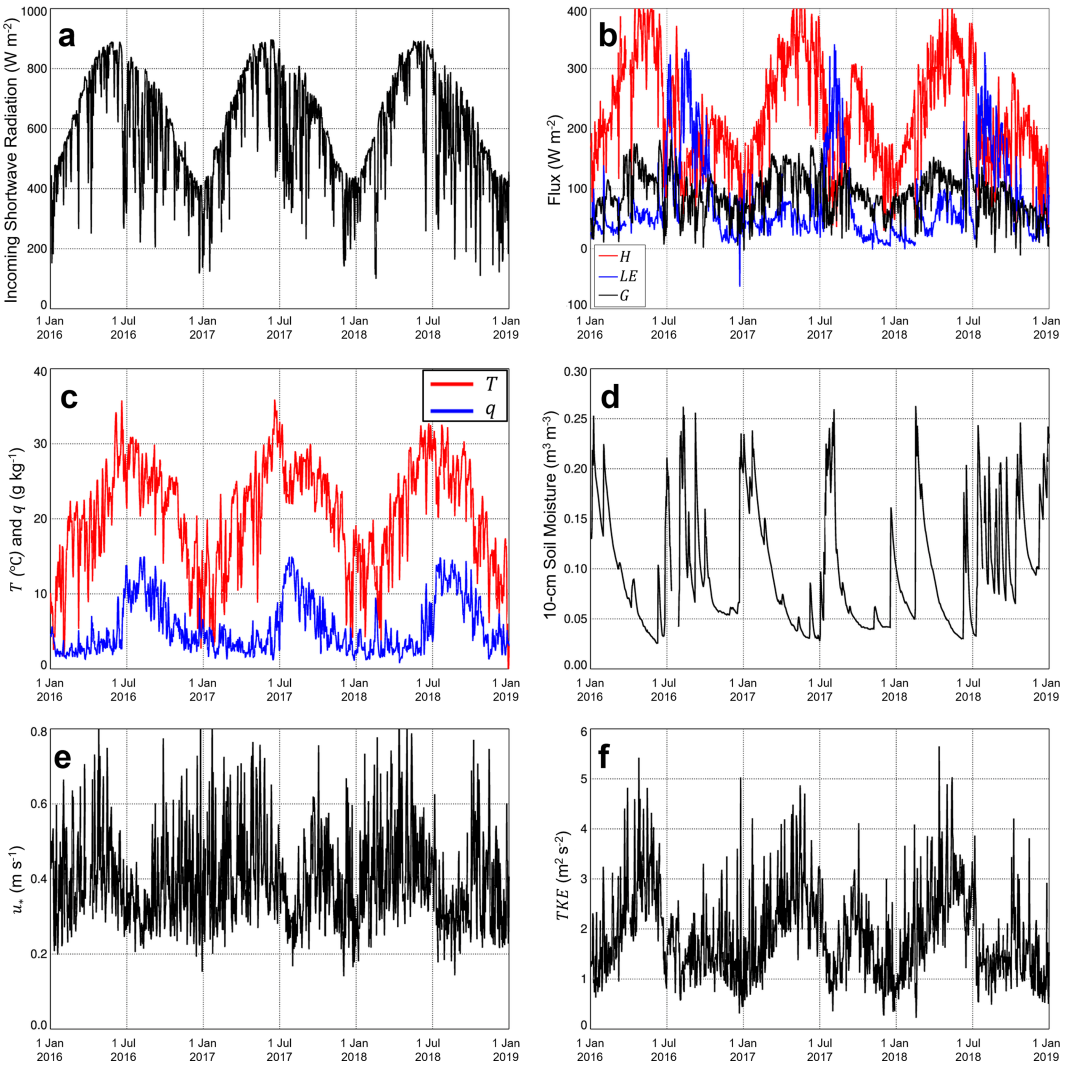

FIG. 4. (a) Mean daytime (0800–1600 LST) incoming shortwave radiation between 1 Jan 2016 and 2019. In (b), mean daytime H (red line), LE (blue line), and G (black line) sampled at Audubon are plotted as a function of time of day between 1 Jan 2016 and 2019. As in (c), but for air temperature (T; red line) and specific humidity (q; blue line). (d)–(f) The mean daytime (0800–1600 LST) 10-cm SM, mean daytime u_*, and mean daytime TKE, respectively, over the time period of interest.

had a maximum value of about 900 W m^{-2} in June (Fig. 4a). Mean daytime H was generally larger than LE throughout the year, with maximum mean daytime H between 300 and 400 W m^{-2} (Fig. 4b). The ground heat flux was a nontrivial term in the SEB, comprising about 25% of the total SEB at Audubon. Regardless, we found excellent agreement (not shown) between the observed net radiation R_{net}, computed as the difference between incoming and outgoing shortwave radiation and longwave radiation, and the sum of H, LE, and G, whereby G is the ground heat flux and the other variables have been defined previously. We found about 91% SEB closure, with an R^2 of 0.96. These values are slightly larger than findings reported during previous years at the study site (i.e., Krishnan et al. 2012), likely because the H and LE datasets used in the present study were tilt-corrected (e.g., Wilczak et al. 2001).

For about 1–2 months beginning around the first week of July when the North American monsoon typically begins (e.g., Carleton 1985), LE exceeded H (Fig. 4b), and mean daytime LE at times exceeded 300 W m^{-2}. For instance, early July was characterized by a marked increase in the mean daytime specific humidity (Fig. 4c) and an increase in SM (Fig. 4d). Premonsoon specific humidity was almost always less than 5 g kg^{-1}, but for the 1–2 months during the monsoon, these values exceeded 10 g kg^{-1}. Mean daytime values of both u_* and TKE exhibited their largest values, of up to about 0.8 m s^{-1} and 4.5 m^2 s^{-2}, respectively, in the premonsoon but markedly decreased upon the monsoon's arrival before slowly returning to premonsoon values (Figs. 4e,f).

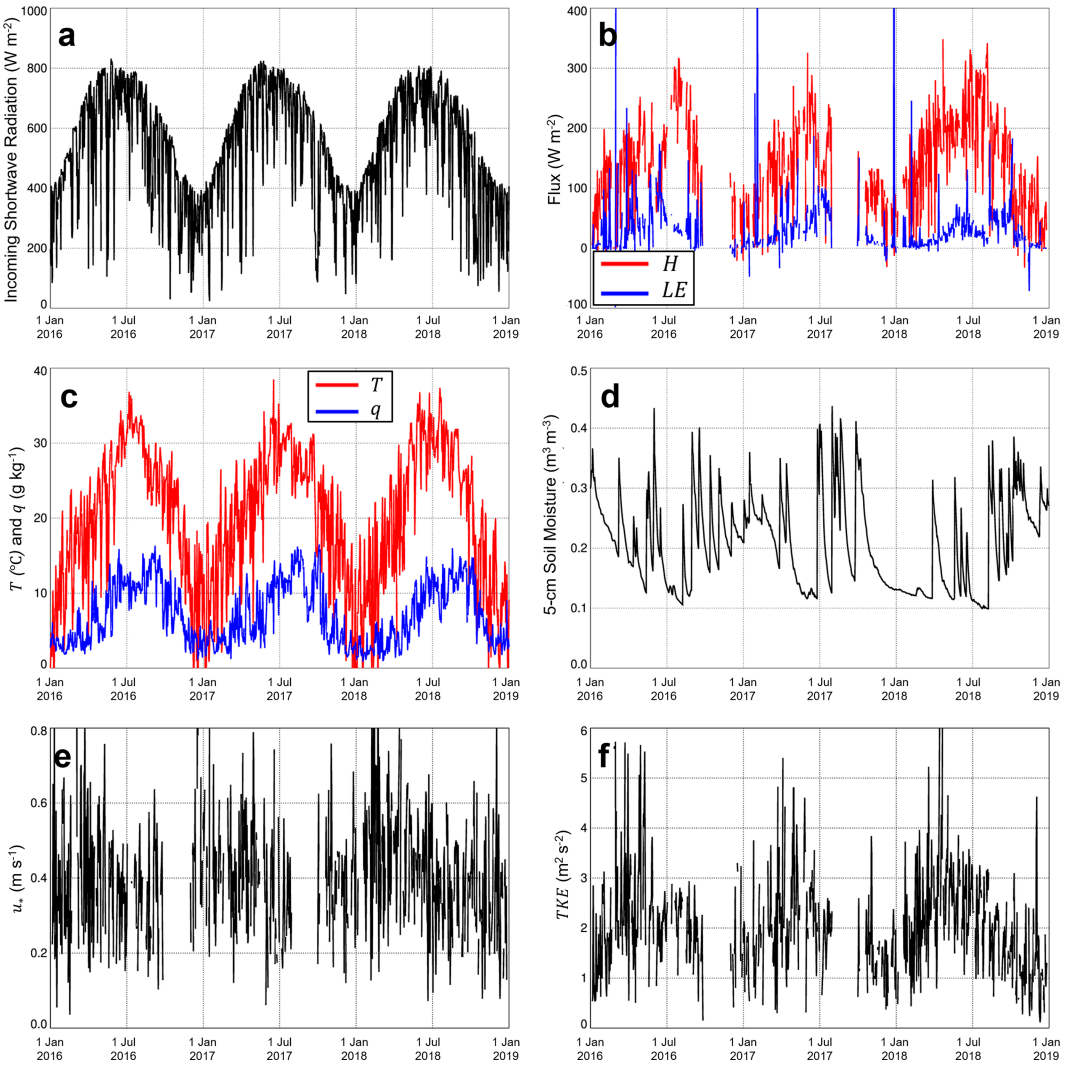

FIG. 5. (a) Mean daytime (0800–1600 LST) incoming shortwave radiation from the WTM site at the RTC between 1 Jan 2016 and 2019. In (b), mean daytime H (red line) and LE (blue line) sampled 10 m AGL at the RTC are plotted as a function of time of day between 1 Jan 2016 and 2019. As in (c), but for air temperature (T; red line) and specific humidity (q; blue line). (d)–(f) The mean daytime 5-cm SM from the WTM site, mean daytime u_* sampled 10 m AGL at the RTC, and mean daytime TKE sampled 10 m AGL at the RTC, respectively, over the time period of interest. Note that H, LE, u_*, and TKE have missing data throughout much of October and November 2016, as well as in August and September 2017.

Based on long-term climatological observations from the collocated long-term climate monitoring site at Audubon, the years 2016, 2017, and 2018 were near normal. The mean annual temperature anomaly from the mean computed over the 20-yr period from 2003 through 2022 was +0.02°, +0.85°, and +0.35°C in 2016, 2017, and 2018, respectively. Precipitation anomalies, computed over the same 20-yr period, were +4.7, −12.5, and +4.5 cm in 2016, 2017, and 2018, respectively.

2) TEXAS SITE

During the 3-yr study period at the RTC, mean incoming shortwave radiation, observed at the nearby WTM site, peaked around 800 W m^{-2} (Fig. 5a). Maximum mean daytime values of H ranged from approximately 100 W m^{-2} in the cool season to as much as 300 W m^{-2} during the middle and late summer (Fig. 5b). Unlike at Audubon, at the RTC, there was no impact of the North American monsoon during the study period. Mean daytime values of LE peaked around 100 W m^{-2} during the summer but almost always remained lower than H. Mean daytime temperatures and specific humidity generally ranged from about 0° to 35°C and from ~3 to ~12 g kg^{-1}, respectively (Fig. 5c). SM exhibited considerably more variability throughout the year (Fig. 5d) than Audubon because the RTC was more impacted by synoptic-scale weather systems (Clark et al. 2022; Anand and Pal 2023). The magnitude of mean daytime values of both u_* and TKE was

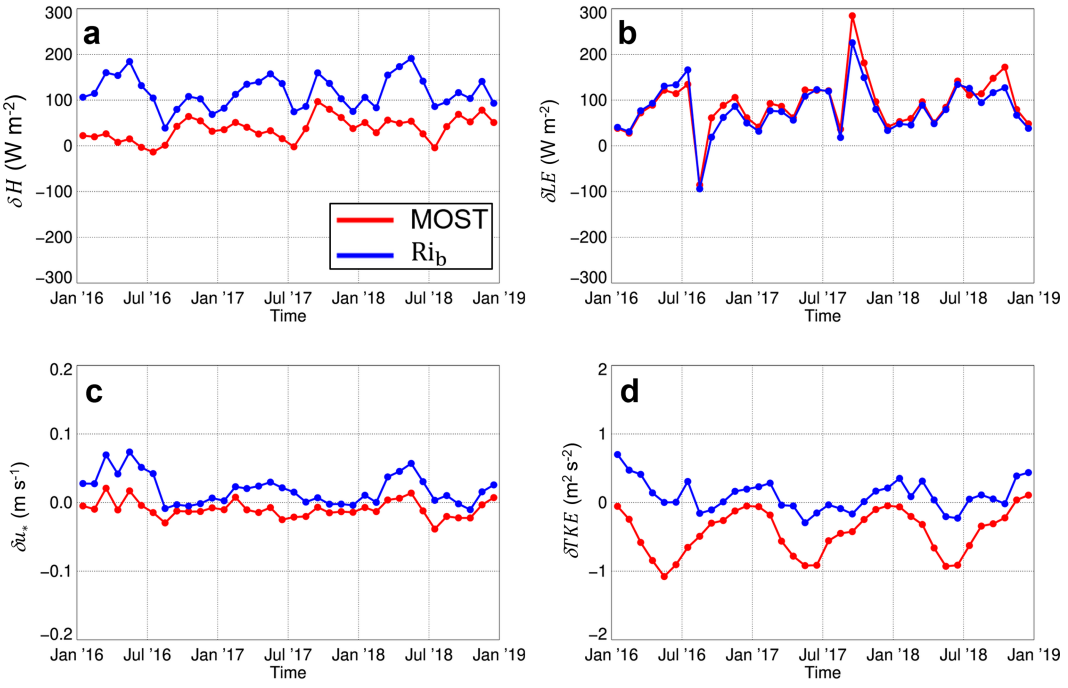

FIG. 6. Mean monthly daytime (0800–1600 LST): (a) δH, (b) δLE, (c) δu_*, and (d) δTKE at Audubon between 1 Jan 2016 and 2019 for the MOST parameterizations (red line) and Richardson parameterizations (blue line).

comparable with those at Audubon and ranged from about 0.2 to 0.7 m s^{-1} and from 1 to –4 m^2 s^{-2} throughout the year (Figs. 5e,f).

To illustrate how the observations from the RTC from the 3-yr period of interest compared against the longer-term climate variability in the region, we used long-term observations from the region. We found that mean annual temperatures were slightly above the 20-yr mean, as the mean annual temperatures in 2016, 2017, and 2018 were +1.06°, +1.06°, and +0.56°C, respectively. 2016 was considerably drier than the long-term mean. About 34.2 cm of rainfall was observed, compared with the 20-yr mean of 47.9 cm. In 2017 and 2018, total precipitation was +7.88 and −9.09 cm, respectively, different from the 20-yr mean.

b. *Efficacy of the MOST and Ri$_b$ parameterizations as a function of time of year*

1) ARIZONA SITE

Over the 3-yr study period at Audubon, δH was typically larger for the Richardson parameterizations than for the MOST parameterizations, and there was a notable seasonal cycle to these biases (Fig. 6a). The largest δH exceeded 100 W m^{-2} in the Richardson parameterizations under dry conditions. In these instances, the maximum observed H was around 300 W m^{-2} but upward of 450 W m^{-2} in the Richardson parameterizations. These conditions were the most common premonsoon but decreased at the monsoon's onset. This decrease also coincided with a δLE decrease (Fig. 6b). Values of δLE were generally positive throughout the year but became negative during the monsoon, with the largest negative biases in δLE occurring during the 2016 and 2017 monsoons. Mean daytime δu_* and δTKE were typically largest premonsoon in the Richardson parameterizations (Figs. 6c,d). In general, the Richardson parameterizations had a positive u_* and TKE bias throughout the year. Biases in the MOST parameterizations for these quantities were negative, and the most negative biases in the MOST parameterizations exceeded 1 m^2 s^{-2} premonsoon.

2) TEXAS SITE

The annual variability in mean daytime δH for MOST and Richardson parameterizations, in general, exhibited a positive bias during the cool season and a negative bias during the warm season (Fig. 7a). Unlike at Audubon, though, the magnitude of mean daytime δH was smaller for the Richardson parameterizations than for the MOST parameterizations. Mean daytime δLE was comparable between the two parameterizations and was typically most negative during the warm season (Fig. 7b). During this time, the errors were quite large and highlight some of the difficulties obtaining reliable parameterized moisture fluxes (e.g., Lee and Buban 2020; Lee et al. 2021). The magnitudes of the mean daytime δu_* were larger at the RTC than at Audubon, but there was little seasonal or interannual variability in δu_*, and the biases were oftentimes larger for the Richardson parameterizations than for the MOST parameterizations (Fig. 7c). Mean daytime δTKE was also larger at the RTC than at Audubon, and the Richardson parameterizations generally had a positive bias, whereas the MOST parameterizations had a negative bias (Fig. 7d).

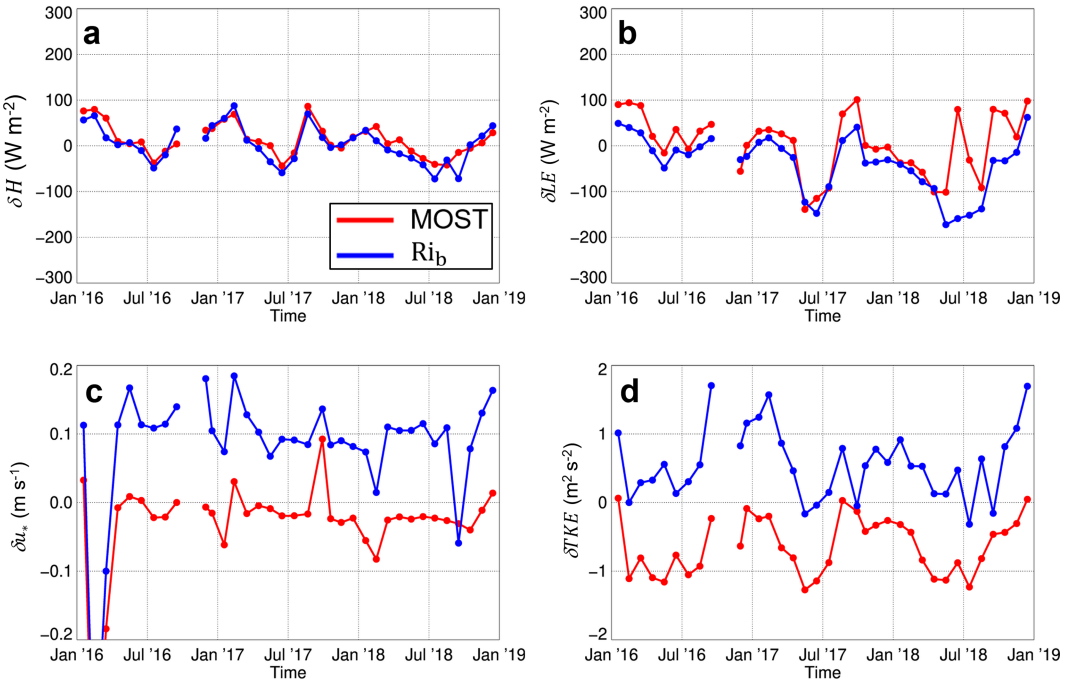

FIG. 7. Mean monthly daytime (0800–1600 LST): (a) δH, (b) δLE, (c) δu_*, and (d) δTKE at the RTC between 1 Jan 2016 and 2019 for the MOST parameterizations (red line) and Richardson parameterizations (blue line).

When we compare the findings from the two sites, we find that the errors in the Richardson parameterizations and MOST parameterizations are more similar at Audubon than at the RTC. As highlighted in the previous section, these two sites have characteristic differences, despite both being located in arid ecosystems. In particular, the observed differences in the results for both the Richardson and MOST parameterizations were nontrivial for the two kinematic parameters (i.e., u_* and TKE). For example, δu_* and δTKE are more positive in the Richardson parameterizations than in the MOST parameterizations at both sites. There is also evidence of the presence of a seasonal cycle in δTKE, which is most pronounced and consistent across years for the MOST δTKE. These results most likely suggest the presence of a systematic bias across different years that results in higher absolute biases for the Richardson parameterizations than the MOST parameterizations, as noted in their seasonal amplitudes for Audubon, while the reported absolute biases appeared to be similar for the RTC. The most negative MOST δTKE occurred during the premonsoon at Audubon and from approximately the late winter to early summer at the RTC.

Some of the differences that we find in the efficacy of the parameterizations at Audubon and RTC can be explained by different synoptic-scale processes at the two sites. At the RTC, ABL and SL mixing and turbulence generation are significantly influenced by near-surface mechanical mixing processes due to generally high wind speeds in the region because of RTC's location downwind of the Mexican Plateau. Also, the RTC and the adjacent region are characterized by frequently occurring mesoscale boundaries (which are most common during the spring and early summer), which distinguish maritime, moist tropical air masses from continental dry air masses originating in arid regions in northern Mexico, eastern New Mexico, and western Texas. The various aspects that cumulatively define the weather features and climatological patterns of the site include frequent extreme temperatures (i.e., hot summers and cold winters), high variability in daily temperature ranges, frequent synoptic events, sustained high-wind regimes, high aerosol loading due to dust, low soil moisture caused by low annual precipitation, and severe weather systems associated with dryline passages (e.g., Kimmel et al. 2016; Anand and Pal 2023; Lee et al. 2023b; Das et al. 2024). These characteristic features most likely yielded the observed differences in the errors for both schemes, in particular for the kinematic parameters.

c. *Efficacy of the MOST and Ri$_b$ parameterizations as a function of Bowen ratio*

1) ARIZONA SITE

Discussion so far of the parameterizations' efficacy has focused on how the errors vary during the 3-yr study period but has not noted the parameterizations' efficacy under varying near-surface micrometeorological conditions. As was shown at Audubon, there were considerable differences in δH and δLE premonsoon as compared with during the monsoon. Therefore, we evaluated how the efficacy of the MOST and Richardson parameterizations varied with ambient surface moisture conditions using the different β quintiles introduced in section 4b. We found that δH and H RMSE at Audubon for MOST parameterizations were consistently lower than the Richardson parameterizations across all β quintiles (Figs. 8a,b).

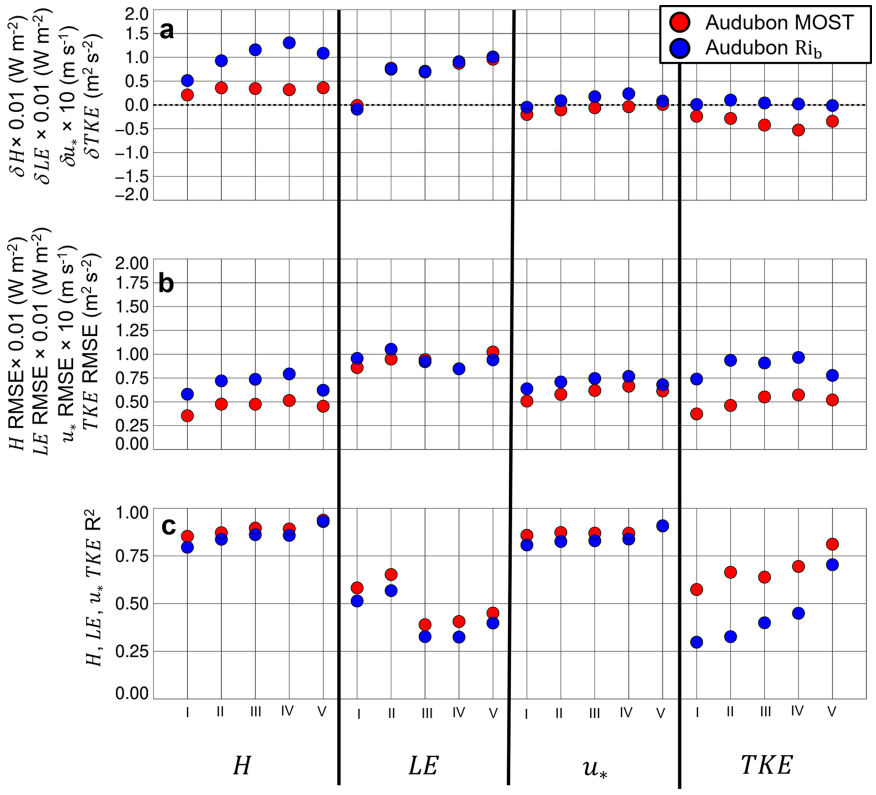

FIG. 8. (a) MBE, (b) RMSE, and R^2 between the MOST-parameterized (red circles) and Ri$_b$-parameterized (blue circles) values of H, LE, u_*, and TKE for the five different β quintiles, whereby I, II, III, IV, and V correspond with the <20th, 20th–40th, 40th–60th, 60th–80th, and >80th percentiles, respectively, at Audubon using on-site observations between 1 Jan 2016 and 31 Dec 2018. To show all statistics on the same graph, the MBE and RMSE for H and LE have been multiplied by 0.01 W m^{-2}, and the MBE and RMSE for u_* have each been multiplied by 10 m s^{-1}. The MBE and RMSE for H and LE have units of watts per square meter; the u_* MBE and u_* RMSE have units of meters per second; and the TKE MBE and RMSE both have units of meters squared per seconds squared. Vertical black lines are used to separate among the different variables.

The term δH for the lowest β quintile (i.e., moist near-surface conditions) for the MOST (Richardson) H was 26 W m^{-2} (64 W m^{-2}) and generally increased as a function of increasing β such that the largest β (i.e., for relatively drier surface conditions) had δH of 50 W m^{-2} (151 W m^{-2}).

Under moist conditions (i.e., instances with the smallest β), δLE for the MOST and Richardson parameterizations were fairly small, i.e., 3 and −5 W m^{-2}, respectively. The δLE for the other β quintiles were considerably larger and were largest for the largest β quintiles, whereby δLE was 155 and 139 W m^{-2}, for the MOST and Richardson parameterizations respectively. The δu_* and RMSE for both the MOST and Richardson parameterizations generally increased as a function of β. The term δu_* ranged from −0.022 to 0.001 m s^{-1} and from −0.0002 to 0.02 m s^{-1} from the smallest β to the largest β for the MOST and Richardson parameterizations, respectively. The δTKE had a negative bias for the MOST parameterization and generally decreased as β increased, whereas δTKE for the Richardson parameterization showed relatively little β dependence.

The values for R^2 were the largest for the MOST and Richardson parameterizations of H and u_*, but here as well as in the LE and TKE parameterizations, R^2 was larger for the MOST parameterizations than for the Richardson parameterizations (Fig. 8c). The difference in R^2 was the largest for the TKE parameterizations, as the MOST parameterizations showed better performance than the Richardson parameterizations across all β quintiles. Whereas R^2 increased as a function of β for the TKE parameterizations, R^2 for the LE parameterizations varied considerably between small β and large β. When β was small, R^2 was around 0.5, but decreased to <0.25 above the ~50th β percentile for both the MOST and Richardson parameterizations.

These findings indicate that both of these parameterizations perform better under more moist near-surface conditions (i.e., relatively lower β and relatively larger LE) than under drier conditions (i.e., relatively larger β and relatively smaller LE). These results are in agreement with Wulfmeyer et al. (2023) who found that the MOST and Richardson parameterizations' prediction of LE was suboptimal compared against

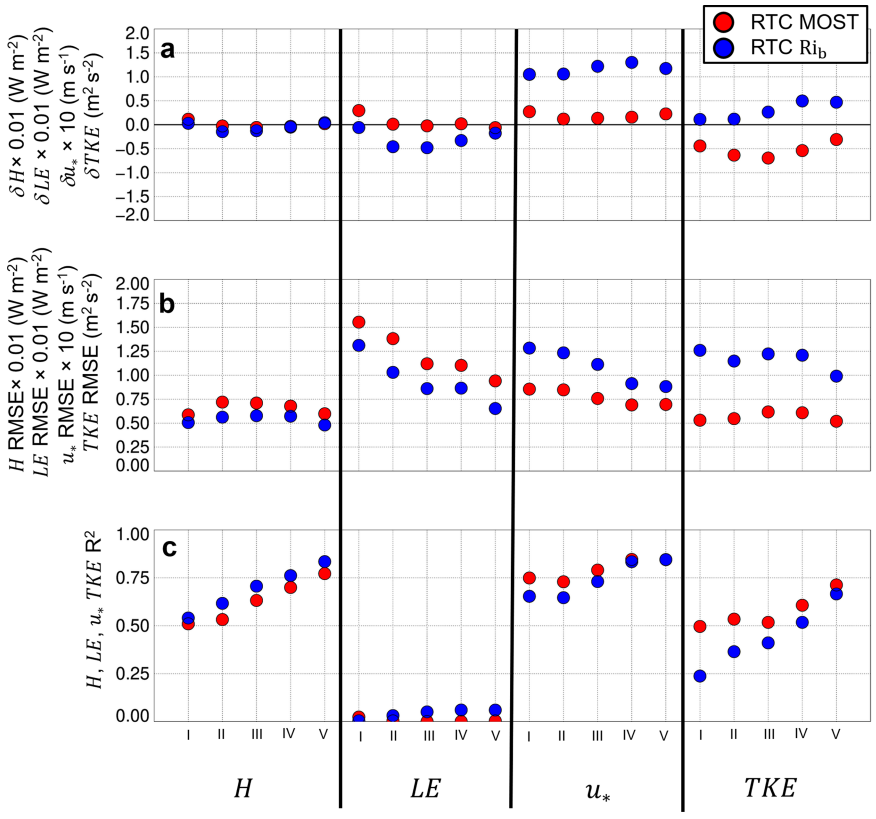

FIG. 9. As in Fig. 8, but for RTC.

their prediction of H and u_*. Similarly, Lee et al. (2023b) found that the MOST and Richardson parameterizations for H struggled under dry conditions when both H and β were large. In contrast, however, Martí et al. (2022) noted the MOST parameterizations for H had difficulty under moist conditions.

2) TEXAS SITE

At the RTC, we found that δH showed little dependence as a function of β. The term δH was quite similar for the MOST and Richardson parameterizations, as δH for the lowest β quintile for the MOST parameterization (Richardson parameterization) was 15.8 W m^{-2} (0.39 W m^{-2}), and for the highest β quintile, the MBE for the MOST parameterization (Richardson parameterization) was 4.7 W m^{-2} (1.7 W m^{-2}) (Fig. 9a). Similarly, the RMSEs exhibited little dependence on β and were around 77 W m^{-2} for the MOST parameterization and 63 W m^{-2} for the Richardson parameterization (Fig. 9b). Whereas the MBEs and RMSEs for the H parameterizations showed little dependence on β, R^2 increased as β increased, and R^2 was larger for the Richardson parameterization than for the MOST parameterization (Fig. 9c).

The δLE for the MOST and Richardson parameterizations generally increased with β (Fig. 9a) but had a negative bias across all β quintiles. The absolute biases were larger for the Richardson than for the MOST parameterizations, with negative biases of up to around 80 W m^{-2} for the lower β values. However, there was large variability within these values, as standard deviations were about 2–3 times larger than the standard deviations for the H parameterizations, resulting in low R^2 (Fig. 9c), which contributed to smaller RMSEs for the Richardson than for the MOST parameterizations of LE for all β quintiles (cf. Fig. 9b). The low R^2 are comparable with values reported in previous work evaluating the efficacy of the MOST and Richardson parameterizations for LE over other areas (e.g., Lee et al. 2021). Difficulties parameterizing LE have been reported to arise due to land surface heterogeneities (e.g., Detto et al. 2008) and moisture advection (e.g., Lee et al. 2004), which are processes that are not directly represented within the moisture parameterizations themselves. Given the relative homogeneity of the area surrounding RTC, we expect advection, rather than land surface heterogeneities, to have a larger impact on the efficacy of the parameterizations at this particular site.

Although the Richardson parameterizations of H and LE at the RTC performed better than the MOST parameterizations for H and LE, based on the lower RMSEs and larger R^2 in the Richardson parameterizations as compared with the MOST parameterizations, the efficacy of the MOST u_* and MOST TKE parameterizations was better than the efficacy of the Richardson u_* and Richardson TKE parameterizations. Both the MOST and Ri$_b$ u_* parameterizations had a mean positive bias, but the bias was larger for the Richardson

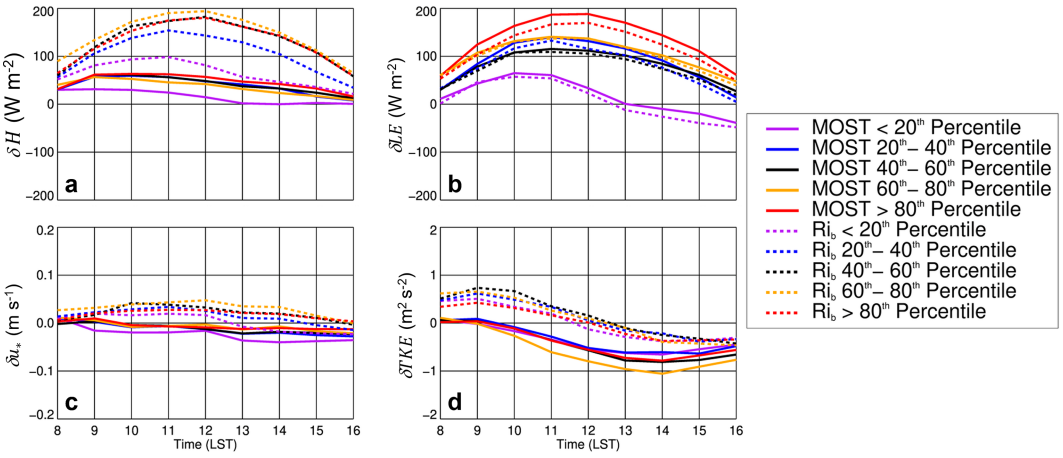

FIG. 10. The (a) δH, (b) δLE, (c) δu_*, and (d) δTKE at Audubon as a function of time of day. Purple, blue, black, orange, and red line indicate the <20th, 20th–40th, 40th–60th, 60th–80th, and >80th percentiles, respectively, of β. The solid and dashed lines are for the MOST and Richardson parameterizations, respectively.

parameterizations across all quintiles of β than for the MOST parameterizations (Fig. 9a). In contrast, the MOST (Richardson) TKE parameterizations had a mean negative (positive) bias across the β quintiles. The RMSEs for the u_* and TKE parameterizations decreased as a function of β but were consistently lower for the MOST parameterizations than for the Richardson parameterizations (Fig. 9b). The R^2 for the MOST and Richardson parameterizations of u_* and TKE increased with increasing β, and R^2 was larger for the MOST parameterizations than for the Richardson parameterizations (Fig. 9c).

d. *Evaluation of parameterizations' efficacy as a function of Bowen ratio: Daytime variability*

1) ARIZONA SITE

The differences we found between the parameterized and observed heat, moisture, and turbulent fluxes occurring as a function of β are further illustrated in the mean diurnal cycles of these differences. In the lowest quintile of β (i.e., moist onsite conditions), mean maximum differences between the MOST parameterizations for H and observed H were around 30 W m^{-2} but ~100 W m^{-2} for the Richardson H parameterizations (Fig. 10a). For the larger β, mean daytime differences between the MOST parameterizations of H and observed H were consistently around 60 W m^{-2}. The Richardson parameterizations of H for the smallest β was maximized around 100 W m^{-2}, but was nearly double this value for the larger values of β. Unlike for the H parameterizations, the Richardson parameterizations performed slightly better than the LE MOST parameterizations for different β (Fig. 10b), and the largest errors in the mean daytime cycles occurred when β was largest.

In case of the u_* parameterizations, the MOST parameterizations had a negative bias of about 0.03 m s^{-1} during the daytime that varied little as a function of ambient moisture conditions, although we note that the largest underestimations occurred during the daytime for the lowest β quintile (Fig. 10c). The Richardson parameterizations showed the opposite pattern, and the differences had larger dependence on β. Although u_* biases in the Richardson parameterizations were positive during the daytime, the bias increased as a function of β.

When evaluating the MOST and Richardson TKE parameterizations as a function of time of day and different β, we found that the magnitude of the negative bias in the MOST TKE parameterizations became larger during the daytime and, in general, increased as a function of β, ranging from about 0.5 m^2 s^{-2} for the smallest β to 1 m^2 s^{-2} for the largest β. The absolute value of the maximum bias also occurred around 1400–1500 LST, whereas maximum bias occurred several hours earlier for the Richardson parameterizations, i.e., 0900–1000 LST. Additionally, the daytime TKE bias in the Richardson parameterization decreased during the daytime, becoming slightly negative during the early afternoon for all β quintiles.

2) TEXAS SITE

When we evaluated the parameterizations as a function of β and time of day at the RTC, we found that the H and LE parameterizations showed little dependence on β across the different β quintiles, and there was generally a mean negative daytime bias for H and LE parameterizations (Figs. 11a,b). Furthermore, δLE was typically negative during the daytime for all β quintiles, and the magnitude of this bias was larger for the Richardson parameterizations than for the MOST parameterizations. As we showed earlier, there was a positive daytime bias in the u_* Richardson parameterizations that was considerably larger than δu_* for the MOST parameterizations. The positive daytime bias in the Richardson parameterizations was consistent with what we found at Audubon, but the bias was larger at the RTC than at Audubon. The analyses of δu_* as a function of time of day indicate that this bias, of about 0.1 m s^{-1}, is present throughout the daytime and does not largely vary as a function of the different β quintiles

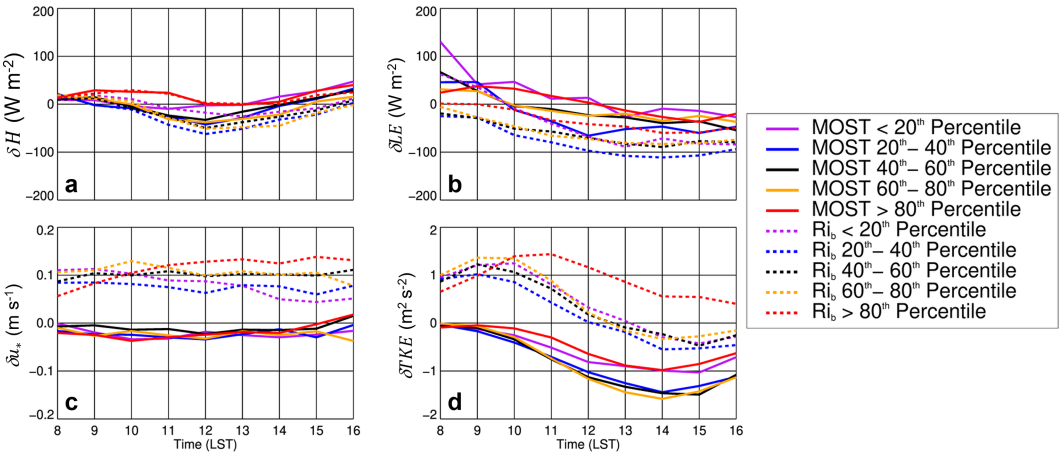

FIG. 11. As in Fig. 10, but for RTC.

(Fig. 11c). The Richardson parameterizations for TKE also had a positive bias, and this bias was largest between 0800 and 1200 LST for all β quintiles. The magnitude of this mid- to late morning maximum increased as a function of β, as it was $\sim$1 m^2 s^{-2} for the lowest β (i.e., moist conditions), but $\sim$1.5 m^2 s^{-2} for the largest β quintiles (i.e., moist conditions, Fig. 11d). Additionally, the MOST parameterizations of TKE had a negative bias present throughout the day. The absolute value of this bias was largest a few hours later than the maximum MBE for the Richardson parameterizations, and its magnitude was similar to the magnitude of the MBE for the Richardson parameterizations of TKE.

e. *Parameterization efficacy when $\beta < 1$ and $\beta > 1$*

Differentiating between regimes in which $\beta < 1$ (i.e., comparatively moist) from regimes in which $\beta > 1$ (i.e., comparatively dry) allows us to investigate the local dependence of the parameterizations' efficacy on β irrespective of the site-specific β quintile. We found that the mean cycle in δH, δLE, δu_*, and δTKE for the MOST and Ri$_b$ parameterizations under conditions when $\beta < 1$ agreed well with our findings reported in the previous section for the smallest β quintiles at both Audubon (Fig. 12) and at the RTC (Fig. 13). The same was true for when $\beta > 1$, which generally represents the average of the second through the fifth quintiles. When $\beta > 1$, the δH, δLE, δu_*, and δTKE mean diurnal cycle for the MOST and Ri$_b$ parameterizations agreed well with the mean diurnal cycle in δH, δLE, δu_*, and δTKE for the MOST and Ri$_b$ parameterizations for the largest β quintiles at both sites.

Furthermore, at Audubon, δLE exceeded 100 W m^{-2} when $\beta > 1$ (and thus LE was by definition smaller than when $\beta < 1$), which results in the decrease in the correlations shown in Fig. 8 when going from lower to higher values of β. The effect was also seen, although to a lesser extent, in δH at Aubudon, as δH increased by about 50 W m^{-2} from $\beta < 1$ (and comparatively smaller H) to $\beta > 1$ (and comparatively larger H) (Figs. 12a,b). The impact of going from $\beta < 1$ to $\beta > 1$ on δH and δLE was more muted at the RTC (Figs. 13a,b). At both sites, δu_* and δTKE did not depend on if $\beta < 1$ or if $\beta > 1$ (Figs. 12c,d and 13c,d).

6. Summary and conclusions

In this study, we used 3 years of meteorological and flux observations obtained from two long-term monitoring sites located in semiarid climate regimes in the southwestern United States to investigate how the efficacy of different SL parameterizations for heat, moisture, and turbulent fluxes varies as a function of different near-surface moisture conditions. We distinguished among these conditions using the Bowen ratio.

We found that, when averaged between 0800 and 1600 LST, the MOST H parameterizations performed better than the Richardson H at Audubon, based on the former having lower RMSE and larger R^2 across the different β quintiles. The opposite was true for the H parameterizations at the RTC, where the Richardson H parameterizations performed better than the MOST parameterizations for H. Furthermore, our results showed that, at Audubon, R^2 for LE decreased from 0.5 to <0.25 from very low values of β (i.e., relatively moist surface conditions, i.e., regimes I and II) to very high values of β (i.e., relatively dry surface conditions, i.e., regimes III, IV, and V). This phenomenon is classically explained by the absence of soil moisture, yielding larger H and, consequently, larger β. On the other hand, one also should note regimes II, III, IV, and V β for both sites (cf. Tables 1 and 2); the median β for regime II for the RTC site was actually close to regime III at Audubon, which also partly explains the lower R^2 values for LE for all regimes. Furthermore, at both Audubon and RTC, the MOST parameterizations better represented u_* and TKE than the Richardson parameterizations.

On diurnal time scales, the H and LE biases increased as a function of increasing β at Audubon, but this pattern was largely absent from the RTC during the study period. At Audubon, the MOST parameterizations had a negative daytime bias, whereas this pattern was opposite and was of the same magnitude for the Richardson parameterizations. At the RTC, the u_* MOST parameterizations generally had a negative bias

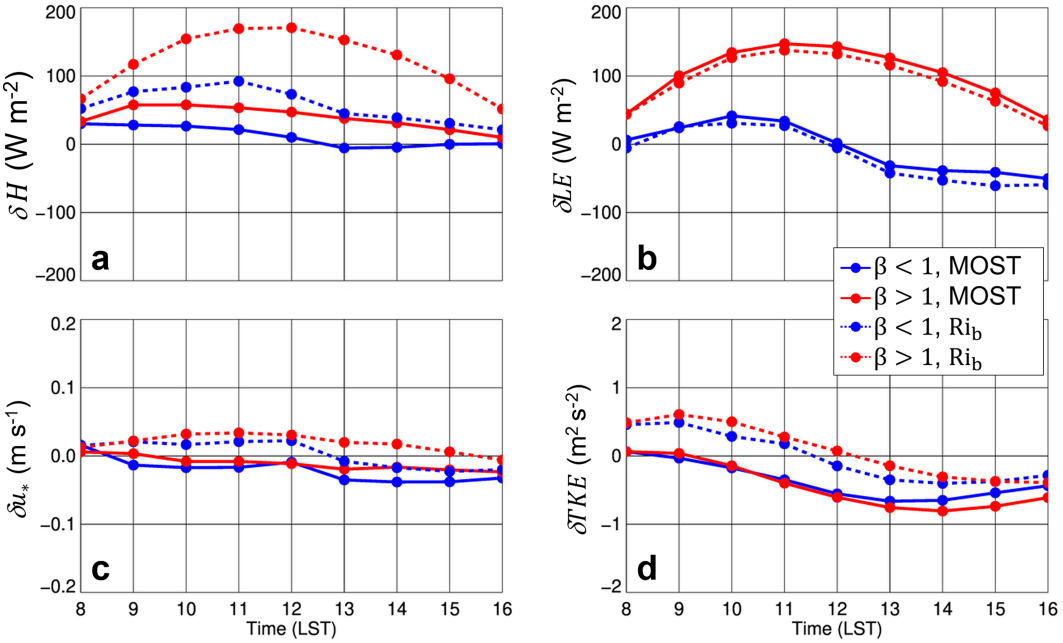

FIG. 12. The (a) δH, (b) δLE, (c) δu_*, and (d) δTKE at Audubon as a function of time of day. Blue and red lines indicate when $\beta < 1$ and $\beta > 1$, respectively. The solid and dashed lines are for the MOST and Richardson parameterizations, respectively.

present throughout the day, but the u_* Richardson parameterizations generally had a positive bias. In both instances, these biases showed little β dependence. The MOST TKE parameterizations had a negative daytime bias at both sites, but the absolute value of this bias was larger at Audubon than at the RTC. At the RTC, the bias generally remained positive throughout the daytime and, as with Audubon, the bias did not vary with β.

We conclude that the efficacy of MOST and Richardson-based SL parameterizations does not strongly vary as a function of β because the impact on β was nearly the same for both of these SL parameterizations. This finding was evident

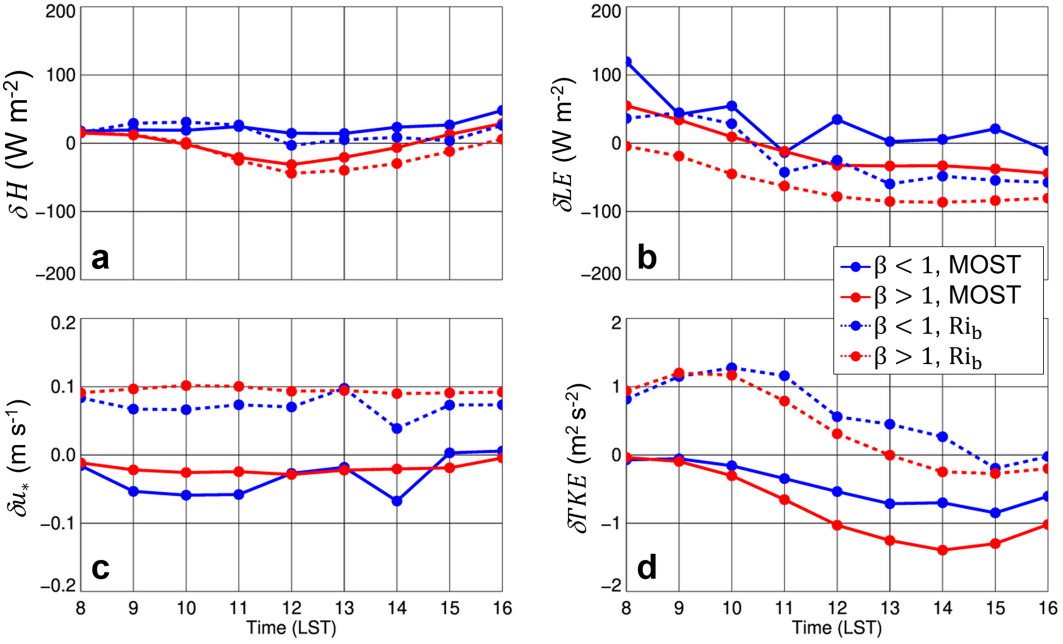

FIG. 13. As in Fig. 12, but for RTC.

by the absence of a consistent relationship between the respective parameterizations' efficacy and β. Furthermore, the results from the two sites suggest that the parameterizations' efficacy is largely site-specific. Tuning the empirically derived fitting coefficients referenced in section 2, as well as quantities such as the heat roughness length (i.e., z_{0h}) to specific sites, and surface moisture regimes, is the possible next step to follow up on this work.

Overall, the findings are consistent with previous work in the literature, highlighting contrasting findings with respect to the performance of SL parameterizations in moist versus dry near-surface conditions (i.e., Martí et al. 2022; Lee et al. 2023b). Furthermore, this also indicates that caution is needed when Richardson-based SL parameterizations are applied to semiarid climatic regimes, based on the efficacy of Ri_b SL parameterizations compared with the MOST-derived SL parameterizations.

Acknowledgments. We greatly appreciate the work by the engineers and technicians from the NOAA Air Resources Laboratory (ARL) Atmospheric Turbulence and Diffusion Division for helping to maintain the flux and meteorological measurements at Audubon, as well as the staff members from Texas Tech University for the monitoring and maintenance of the RTC measurements. We also thank Mr. Matthew Asel and Mr. Wesley Burgett from the National Wind Institute at Texas Tech University for assisting with providing the RTC measurements and for aiding in their interpretation. Co-author Sandip Pal was partially supported by the NOAA Grant NA21OAR4590361. We greatly appreciate the efforts of three anonymous reviewers whose comments and suggestions helped us strengthen the presentation and scientific content of this manuscript, and we thank the anonymous reviewer from NOAA ARL for suggestions on an earlier version of the manuscript. Finally, the results and conclusions obtained from this work, as well as any views that we expressed herein, are those of the authors and may not necessarily reflect the views of NOAA or the Department of Commerce.

Data availability statement. The high-frequency datasets that were used to calculate the 30-min fluxes and turbulence statistics from the Audubon and RTC, as well as the WTM datasets, are available upon request from the corresponding author. The digital elevation model used to help generate Fig. 1 was obtained from the PRISM climate group and may be accessed at https://prism.oregonstate.edu/downloads/.

REFERENCES

Anand, M., and S. Pal, 2023: Exploring atmospheric boundary layer depth variability in frontal environments over an arid region. *Bound.-Layer Meteor.*, **186**, 251–285, https://doi.org/10.1007/s10546-022-00756-z.

Andreas, E. L., and B. B. Hicks, 2002: Comments on "critical test of the validity of Monin–Obukhov similarity during convective conditions". *J. Atmos. Sci.*, **59**, 2605–2607, https://doi.org/10.1175/1520-0469(2002)059<2605:COCTOT>2.0.CO;2.

Baldocchi, D., K. Novick, T. Keenan, and M. Torn, 2024: AmeriFlux: Its impact on our understanding of the 'breathing of the biosphere', after 25 years. *Agric. For. Meteor.*, **348**, 109929, https://doi.org/10.1016/j.agrformet.2024.109929.

Benjamin, S. G., and Coauthors, 2016: A North American hourly assimilation and model forecast cycle: The Rapid Refresh. *Mon. Wea. Rev.*, **144**, 1669–1694, https://doi.org/10.1175/MWR-D-15-0242.1.

Berg, A., and Coauthors, 2016: Land–atmosphere feedbacks amplify aridity increase over land under global warming. *Nat. Climate Change*, **6**, 869–874, https://doi.org/10.1038/nclimate3029.

Bhowmick, M., and D. J. Parker, 2018: Analytical solution to a thermodynamic model for the sensitivity of afternoon deep convective initiation to the surface Bowen ratio. *Quart. J. Roy. Meteor. Soc.*, **144**, 2216–2229, https://doi.org/10.1002/qj.3340.

Billesbach, D. P., 2011: Estimating uncertainties in individual eddy covariance flux measurements: A comparison of methods and a proposed new method. *Agric. For. Meteor.*, **151**, 394–405, https://doi.org/10.1016/j.agrformet.2010.12.001.

Businger, J. A., J. C. Wyngaard, Y. Izumi, and E. F. Bradley, 1971: Flux-profile relationships in the atmospheric surface layer. *J. Atmos. Sci.*, **28**, 181–189, https://doi.org/10.1175/1520-0469(1971)028<0181:FPRITA>2.0.CO;2.

Byun, D. W., 1990: On the analytical solutions of flux-profile relationships for the atmospheric surface layer. *J. Appl. Meteor.*, **29**, 652–657, https://doi.org/10.1175/1520-0450(1990)029<0652:OTASOF>2.0.CO;2.

Carleton, A. M., 1985: Synoptic and satellite aspects of the southwestern U.S. summer 'monsoon'. *J. Climatol.*, **5**, 389–402, https://doi.org/10.1002/joc.3370050406.

Clark, N. E., S. Pal, and T. R. Lee, 2022: Empirical evidence for the frontal modification of atmospheric boundary layer depth variability over land. *J. Appl. Meteor. Climatol.*, **61**, 1041–1063, https://doi.org/10.1175/JAMC-D-21-0099.1.

Das, D. S. Pal, E. Bruning, and B. Hirth, 2024: Exploring spatial variability of precipitation over the semi-arid region of West Texas using ground based and satellite remote sensing measurements synergy. *IGARSS 2024—2024 IEEE Int. Geoscience and Remote Sensing Symp.*, Athens, Greece, Institute of Electrical and Electronics Engineers, 5662–5665, https://doi.org/10.1109/IGARSS53475.2024.10641391.

Detto, M., G. Katul, M. Mancini, N. Montaldo, and J. D. Albertson, 2008: Surface heterogeneity and its signature in higher-order scalar similarity relationships. *Agric. For. Meteor.*, **148**, 902–916, https://doi.org/10.1016/j.agrformet.2007.12.008.

Diamond, H. J., and Coauthors, 2013: U.S. Climate Reference Network after one decade of operations: Status and assessment. *Bull. Amer. Meteor. Soc.*, **94**, 485–498, https://doi.org/10.1175/BAMS-D-12-00170.1.

Dowell, D. C., and Coauthors, 2022: The High-Resolution Rapid Refresh (HRRR): An hourly updating convection-allowing forecast model. Part 1: Motivation and system description. *Wea. Forecasting*, **37**, 1391–1395, https://doi.org/10.1175/WAF-D-21-0151.1.

Dyer, A. J., 1974: A review of flux-profile relationships. *Bound.-Layer Meteor.*, **7**, 363–372, https://doi.org/10.1007/BF00240838.

Findell, K. L., and E. A. B. Eltahir, 2003: Atmospheric controls on soil moisture–boundary layer interactions. Part I: Framework development. *J. Hydrometeor.*, **4**, 552–569, https://doi.org/10.1175/1525-7541(2003)004<0552:ACOSML>2.0.CO;2.

Friedrich, K., N. Mölders, and G. Tetzlaff, 2000: On the influence of surface heterogeneity on the Bowen-ratio: A theoretical case study. *Theor. Appl. Climatol.*, **65**, 181–196, https://doi.org/10.1007/s007040070043.

Greene, B. R., S. T. Kral, P. B. Chilson, and J. Reuder, 2022: Gradient-based turbulence estimates from multicopter profiles in the Arctic stable boundary layer. *Bound.-Layer Meteor.*, **183**, 321–353, https://doi.org/10.1007/s10546-022-00693-x.

Hamel, M. S., 2022: Convective boundary layer turbulence profiling over an arid region using a 200m tall-tower and Doppler lidar measurements. M.S. thesis, Dept. of Geosciences, Texas Tech University, 143 pp., https://ttu-ir.tdl.org/bitstreams/f52ba1b4-95e1-42cd-b3d3-4f1d2bd7c8fc/download.

Hicks, B. B., 1978: Some limitations of dimensional analysis and power laws. *Bound.-Layer Meteor.*, **14**, 567–569, https://doi.org/10.1007/BF00121895.

——, 1981: An examination of turbulence statistics in the surface boundary layer. *Bound.-Layer Meteor.*, **21**, 389–402, https://doi.org/10.1007/BF00119281.

Högström, U., 1996: Review of some basic characteristics of the atmospheric surface layer. *Bound.-Layer Meteor.*, **78**, 215–246, https://doi.org/10.1007/BF00120937.

Huang, J., and Coauthors, 2017: Dryland climate change: Recent progress and challenges. *Rev. Geophys.*, **55**, 719–778, https://doi.org/10.1002/2016RG000550.

James, E. P., and Coauthors, 2022: The High-Resolution Rapid Refresh (HRRR): An hourly updating convection-allowing forecast model. Part II: Forecast performance. *Wea. Forecasting*, **37**, 1397–1417, https://doi.org/10.1175/WAF-D-21-0130.1.

Jiménez, P. A., J. Dudhia, J. F. González-Rouco, J. Navarro, J. P. Montávez, and E. García-Bustamante, 2012: A revised scheme for the WRF surface layer formulation. *Mon. Wea. Rev.*, **140**, 898–918, https://doi.org/10.1175/MWR-D-11-00056.1.

Jin, S., J. Dewitz, P. Danielson, B. Granneman, C. Costello, K. Smith, and Z. Zhu, 2023: National Land Cover Database 2019: A new strategy for creating clean leaf-on and leaf-off landsat composite images. *J. Remote Sens.*, **3**, 0022, https://doi.org/10.34133/remotesensing.0022.

Kannenberg, S. A., W. R. L. Anderegg, M. L. Barnes, M. P. Dannenberg, and A. K. Knapp, 2024: Dominant role of soil moisture in mediating carbon and water fluxes in dryland ecosystems. *Nat. Geosci.*, **17**, 38–43, https://doi.org/10.1038/s41561-023-01351-8.

Kelley, C. L., and B. L. Ennis, 2016: *SWiFT site atmospheric characterization.* SNL-NM Tech. Rep. SAND-2016-0216, 82 pp., https://www.osti.gov/servlets/purl/1237403.

Kimmel, T. M., Jr., J. Nielsen-Gammon, B. Rose, and H. M. Mogil, 2016: The weather and climate of Texas: A big state with big extremes. *Weatherwise*, **69**, 25–33, https://doi.org/10.1080/00431672.2016.1206446.

Konapala, G., A. K. Mishra, Y. Wada, and M. E. Mann, 2020: Climate change will affect global water availability through compounding changes in seasonal precipitation and evaporation. *Nat. Commun.*, **11**, 3044, https://doi.org/10.1038/s41467-020-16757-w.

Krishnan, P., T. P. Meyers, R. L. Scott, L. Kennedy, and M. Heuer, 2012: Energy exchange and evapotranspiration over two temperate semi-arid grasslands in North America. *Agric. For. Meteor.*, **153**, 31–44, https://doi.org/10.1016/j.agrformet.2011.09.017.

Kumar, V., J. Kleissl, C. Meneveau, and M. B. Parlange, 2006: Large-eddy simulation of a diurnal cycle of the atmospheric boundary layer: Atmospheric stability and scaling issues. *Water Resour. Res.*, **42**, W06D09, https://doi.org/10.1029/2005WR004651.

Lamaud, E., and M. Irvine, 2006: Temperature–humidity dissimilarity and heat-to-water-vapour transport efficiency above and within a pine forest canopy: The role of the Bowen ratio. *Bound.-Layer Meteor.*, **120**, 87–109, https://doi.org/10.1007/s10546-005-9032-6.

Lee, T. R., and M. Buban, 2020: Evaluation of Monin–Obukhov and bulk Richardson parameterizations for surface—atmosphere exchange. *J. Appl. Meteor. Climatol.*, **59**, 1091–1107, https://doi.org/10.1175/JAMC-D-19-0057.1.

——, and T. P. Meyers, 2023: New parameterizations of turbulence statistics for the atmospheric surface layer. *Mon. Wea. Rev.*, **151**, 85–103, https://doi.org/10.1175/MWR-D-22-0071.1.

——, M. Buban, D. D. Turner, T. P. Meyers, and C. B. Baker, 2019: Evaluation of the High-Resolution Rapid Refresh (HRRR) model using near-surface meteorological and flux observations from northern Alabama. *Wea. Forecasting*, **34**, 635–663, https://doi.org/10.1175/WAF-D-18-0184.1.

——, M. S. Buban, and T. P. Meyers, 2021: Application of bulk Richardson parameterizations of surface fluxes to heterogeneous land surfaces. *Mon. Wea. Rev.*, **149**, 3243–3264, https://doi.org/10.1175/MWR-D-21-0047.1.

——, R. D. Leeper, T. Wilson, H. J. Diamond, T. P. Meyers, and D. D. Turner, 2023a: Using the U.S. Climate Reference Network to identify biases in near- and subsurface meteorological fields in the High-Resolution Rapid Refresh (HRRR) Weather Prediction model. *Wea. Forecasting*, **38**, 879–900, https://doi.org/10.1175/WAF-D-22-0213.1.

——, S. Pal, P. Krishnan, B. Hirth, M. Heuer, T. P. Meyers, R. D. Saylor, and J. Schroeder, 2023b: On the efficacy of Monin–Obukhov and bulk Richardson surface-layer parameterizations over drylands. *J. Appl. Meteor. Climatol.*, **62**, 855–875, https://doi.org/10.1175/JAMC-D-23-0092.1.

——, ——, R. D. Leeper, T. Wilson, H. J. Diamond, T. P. Meyers, and D. D. Turner, 2024: On the importance of regime-specific evaluations for numerical weather prediction models as demonstrated using the High-Resolution Rapid Refresh (HRRR) model. *Wea. Forecasting*, **39**, 781–791, https://doi.org/10.1175/WAF-D-23-0177.1.

——, and Coauthors, 2025: On the application of the hockey-stick transition hypothesis to characterize turbulence within and above a deciduous forest. *Agric. For. Meteor.*, **362**, 110342, https://doi.org/10.1016/j.agrformet.2024.110342.

Lee, X., Q. Yu, X. Sun, J. Liu, Q. Min, Y. Liu, and X. Zhang, 2004: Micrometeorological fluxes under the influence of regional and local advection: A revisit. *Agric. For. Meteor.*, **122**, 111–124, https://doi.org/10.1016/j.agrformet.2003.02.001.

Lewis, J. M., 1995: The story behind the Bowen ratio. *Bull. Amer. Meteor. Soc.*, **76**, 2433–2443, https://doi.org/10.1175/1520-0477(1995)076<2433:TSBTBR>2.0.CO;2.

Liu, H., C. Liu, J. Huang, A. R. Desai, Q. Zhang, K. Ghannam, and G. G. Katul, 2024: Scalar flux profiles in the unstable atmospheric surface layer under the influence of large eddies: Implications for eddy covariance flux measurements and the non-closure problem. *Geophys. Res. Lett.*, **51**, e2023GL106649, https://doi.org/10.1029/2023GL106649.

Markowski, P. M., N. T. Lis, D. D. Turner, T. R. Lee, and M. S. Buban, 2019: Observations of near-surface vertical wind profiles and vertical momentum fluxes from VORTEX-SE 2017: Comparisons to Monin–Obukhov similarity theory. *Mon. Wea. Rev.*, **147**, 3811–3824, https://doi.org/10.1175/MWR-D-19-0091.1.

Martí, B., D. Martínez-Villagrasa, and J. Cuxart, 2022: Flux–gradient relationships below 2 m over a flat site in complex terrain. *Bound.-Layer Meteor.*, **184**, 505–530, https://doi.org/10.1007/s10546-022-00719-4.

Martínez-Fernández, J., A. González-Zamora, and L. Almendra-Martín, 2021: Soil moisture memory and soil properties: An analysis with the stored precipitation fraction. *J. Hydrol.*, **593**, 125622, https://doi.org/10.1016/j.jhydrol.2020.125622.

Massman, W. J, and X. Lee, 2002: Eddy covariance flux corrections and uncertainties in long-term studies of carbon and energy exchanges. *Agric. For. Meteor.*, **113**, 121–144, https://doi.org/10.1016/S0168-1923(02)00105-3.

Mauder, M., T. Foken, and J. Cuxart, 2020: Surface-energy-balance closure over land: A review. *Bound.-Layer Meteor.*, **177**, 395–426, https://doi.org/10.1007/s10546-020-00529-6.

——, ——, M. Aubinet, and A. Ibrom, 2021: Eddy-covariance measurements. *Springer Handbook of Atmospheric Measurements*, T. Foken, Eds., Springer Handbooks, Springer, 1473–1504, https://doi.org/10.1007/978-3-030-52171-4_55.

Meesters, A. G. C. A., N. J. Bink, E. A. C. Henneken, H. F. Vugts, and F. Cannemeijer, 1997: Katabatic wind profiles over the Greenland ice sheet: Observation and modelling. *Bound.-Layer Meteor.*, **85**, 475–496, https://doi.org/10.1023/A:1000514214823.

Meyers, T. P., 2001: A comparison of summertime water and CO_2 fluxes over rangeland for well watered and drought conditions. *Agric. For. Meteor.*, **106**, 205–214, https://doi.org/10.1016/S0168-1923(00)00213-6.

——, 2016: AmeriFlux BASE US-Aud Audubon Research Ranch, Ver. 4-1. AmeriFlux AMP, accessed 24 November 2023, https://doi.org/10.17190/AMF/1246028.

——, and D. D. Baldocchi, 2005: Current micrometeorological flux methodologies with applications in agriculture. *Micrometeorology in Agricultural Systems*, *Agronomy Monogr.*, No. 47, American Society of Agronomy, Crop Science Society of America, and Soil Science Society of America, 381–396, https://doi.org/10.2134/agronmonogr47.c16.

Monin, A. S., and A. M. Obukhov, 1954: Basic laws of turbulent mixing in the surface layer of the atmosphere. *Tr. Geofiz. Inst., Akad. Nauk SSSR*, **24**, 163–187.

National Academies of Sciences, Engineering, and Medicine, 2018: *The Future of Atmospheric Boundary Layer Observing, Understanding, and Modeling: Proceedings of a Workshop.* The National Academies Press, 58 pp., https://doi.org/10.17226/25138.

Novick, K. A., J. A. Biederman, A. R. Desai, M. E. Litvak, D. J. P. Moore, R. L. Scott, and M. S. Torn, 2018: The AmeriFlux network: A coalition of the willing. *Agric. For. Meteor.*, **249**, 444–456, https://doi.org/10.1016/j.agrformet.2017.10.009.

Pal, S., and M. Haeffelin, 2015: Forcing mechanisms governing diurnal, seasonal, and inter-annual variability in the boundary layer depths: Five years of continuous lidar observations over a suburban site near Paris. *J. Geophys. Res. Atmos.*, **120**, 11 936–11 956, https://doi.org/10.1002/2015JD023268.

——, ——, and E. Batchvarova, 2013: Exploring a geophysical process-based attribution technique for the determination of the atmospheric boundary layer depth using aerosol lidar and near-surface meteorological measurements. *J. Geophys. Res. Atmos.*, **118**, 9277–9295, https://doi.org/10.1002/jgrd.50710.

——, N. E. Clark, M. Anand, and M. Hamel, 2024: Aerosol transport and associated boundary layer thermodynamics under contrasting synoptic conditions over a semiarid site. *Sci. Total Environ.*, **962**, 178357, https://doi.org/10.1016/j.scitotenv.2024.178357.

——, ——, T. R. Lee, M. Conder, and M. Buban, 2021: When and where horizontal advection is critical to alter atmospheric boundary layer dynamics over land: The need for a conceptual framework. *Atmos. Res.*, **264**, 105825, https://doi.org/10.1016/j.atmosres.2021.105825.

Panin, G. N., and G. Tetzlaff, 1999: A measure of inhomogeneity of the land surface and parametrization of turbulent fluxes under natural conditions. *Theor. Appl. Climatol.*, **62**, 3–8, https://doi.org/10.1007/s007040050069.

Prăvălie, R., 2016: Drylands extent and environmental issues. A global approach. *Earth-Sci. Rev.*, **161**, 259–278, https://doi.org/10.1016/j.earscirev.2016.08.003.

Reynolds, J. F., and Coauthors, 2007: Global desertification: Building a science for dryland development. *Science*, **316**, 847–851, https://doi.org/10.1126/science.1131634.

Ripple, W. J., and Coauthors, 2024: The 2024 state of the climate report: Perilous times on planet Earth. *BioScience*, **74**, 812–824, https://doi.org/10.1093/biosci/biae087.

Salesky, S. T., and M. Chamecki, 2012: Random errors in turbulence measurements in the atmospheric surface layer: Implications for Monin–Obukhov similarity theory. *J. Atmos. Sci.*, **69**, 3700–3714, https://doi.org/10.1175/JAS-D-12-096.1.

Sauer, T. J., and R. Horton, 2005: Soil heat flux. *Micrometeorology in Agricultural Systems*, J. L. Hatfield and J. M. Baker, Eds., American Society of Agronomy, 131–154.

Schmidt, A., C. Hanson, W. S. Chan, and B. E. Law, 2012: Empirical assessment of uncertainties of meteorological parameters and turbulent fluxes in the AmeriFlux network. *J. Geophys. Res.*, **117**, G04014, https://doi.org/10.1029/2012JG002100.

Schroeder, J. L., W. S. Burgett, K. B. Haynie, I. Sonmez, G. D. Skwira, A. L. Doggett, and J. W. Lipe, 2005: The West Texas Mesonet: A technical overview. *J. Atmos. Ocean Technol.*, **22**, 211–222, https://doi.org/10.1175/JTECH-1690.1.

Sfyri, E., M. W. Rotach, I. Stiperski, F. C. Bosveld, M. Lehner, and F. Obleitner, 2018: Scalar-flux similarity in the layer near the surface over mountainous terrain. *Bound.-Layer Meteor.*, **169**, 11–46, https://doi.org/10.1007/s10546-018-0365-3.

Sorbjan, Z., 2006: Comments on 'Flux–gradient relationship, self-correlation and intermittency in the stable boundary layer'. *Quart. J. Roy. Meteor. Soc.*, **132**, 1371–1373, https://doi.org/10.1256/qj.05.168A.

——, 2010: Gradient-based scales and similarity laws in the stable boundary layer. *Quart. J. Roy. Meteor. Soc.*, **136**, 1243–1254, https://doi.org/10.1002/qj.638.

——, and A. A. Grachev, 2010: An evaluation of the flux–gradient relationship in the stable boundary layer. *Bound.-Layer Meteor.*, **135**, 385–405, https://doi.org/10.1007/s10546-010-9482-3.

Stiperski, I., and M. Calaf, 2023: Generalizing Monin-Obukhov similarity theory (1954) for complex atmospheric turbulence. *Phys. Rev. Lett.*, **130**, 124001, https://doi.org/10.1103/PhysRevLett.130.124001.

——, ——, and M. W. Rotach, 2019: Scaling, anisotropy, and complexity in near-surface atmospheric turbulence. *J. Geophys. Res. Atmos.*, **124**, 1428–1448, https://doi.org/10.1029/2018JD029383.

Stull, R. B., 1988: *An Introduction to Boundary Layer Meteorology.* Kluwer Academic, 666 pp.

Sun, J., E. S. Takle, and O. C. Acevedo, 2020: Understanding physical processes represented by the Monin–Obukhov bulk

formula for momentum transfer. *Bound.-Layer Meteor.*, **177**, 69–95, https://doi.org/10.1007/s10546-020-00546-5.

Sverdrup, H. U., 1943: On the ratio between heat conduction from the sea surface and heat used for evaporation. *Ann. N. Y. Acad. Sci.*, **44**, 81–88, https://doi.org/10.1111/j.1749-6632.1943.tb31294.x.

Teixeira, J., and Coauthors, 2021: Toward a Global Planetary Boundary Layer Observing System. The NASA PBL Incubation Study Team Rep., 134 pp., https://ntrs.nasa.gov/api/citations/20230001633/downloads/AFridlindPBLTowardsReport.pdf.

Webb, E. K., G. I. Pearman, and R. Leuning, 1980: Correction of flux measurements for density effects due to heat and water vapour transfer. *Quart. J. Roy. Meteor. Soc.*, **106**, 85–100, https://doi.org/10.1002/qj.49710644707.

Wilczak, J. M., S. P. Oncley, and S. A. Stage, 2001: Sonic anemometer tilt correction algorithms. *Bound.-Layer Meteor.*, **99**, 127–150, https://doi.org/10.1023/A:1018966204465.

Wulfmeyer, V., J. M. V. Pineda, S. Otte, M. Karlbauer, M. V. Butz, T. R. Lee, and V. Rajtschan, 2023: Estimation of the surface fluxes for heat and momentum in unstable conditions with machine learning and similarity approaches for the LAFE data set. *Bound.-Layer Meteor.*, **186**, 337–371, https://doi.org/10.1007/s10546-022-00761-2.

Zhuojia, Y., and R. A. Pielke, 1995: Parameterization of Bowen ratio with respect to soil moisture availability. *Adv. Atmos. Sci.*, **12**, 449–474, https://doi.org/10.1007/BF02657005.